

A CRMP4-dependent retrograde axon-to-soma death signal in amyotrophic lateral sclerosis

Roy Maimon^{1,†}, Lior Ankol^{1,2,†}, Tal Gradus Pery¹, Topaz Altman¹, Ariel Ionescu¹, Romana Weissova^{3,4}, Michael Ostrovsky¹, Elizabeth Tank⁵, Gayster Alexandra⁶, Natalia Shelestovich^{1,6}, Yarden Opatowsky⁷, Amir Dori^{1,2,8}, Sami Barmada⁵ , Martin Balastik³  & Eran Perlson^{1,2,*} 

Abstract

Amyotrophic lateral sclerosis (ALS) is a fatal non-cell-autonomous neurodegenerative disease characterized by the loss of motor neurons (MNs). Mutations in CRMP4 are associated with ALS in patients, and elevated levels of CRMP4 are suggested to affect MN health in the SOD1^{G93A}-ALS mouse model. However, the mechanism by which CRMP4 mediates toxicity in ALS MNs is poorly understood. Here, by using tissue from human patients with sporadic ALS, MNs derived from *C9orf72*-mutant patients, and the SOD1^{G93A}-ALS mouse model, we demonstrate that subcellular changes in CRMP4 levels promote MN loss in ALS. First, we show that while expression of CRMP4 protein is increased in cell bodies of ALS-affected MN, CRMP4 levels are decreased in the distal axons. Cellular mislocalization of CRMP4 is caused by increased interaction with the retrograde motor protein, dynein, which mediates CRMP4 transport from distal axons to the soma and thereby promotes MN loss. Blocking the CRMP4-dynein interaction reduces MN loss in human-derived MNs (*C9orf72*) and in ALS model mice. Thus, we demonstrate a novel CRMP4-dependent retrograde death signal that underlies MN loss in ALS.

Keywords ALS; axonal transport; CRMP4; dynein; retrograde signaling

Subject Categories Molecular Biology of Disease; Neuroscience

DOI 10.15252/emj.2020107586 | Received 23 December 2020 | Revised 11 May 2021 | Accepted 28 May 2021 | Published online 30 June 2021

The EMBO Journal (2021) 40: e107586

Introduction

Amyotrophic lateral sclerosis (ALS) is a lethal neurodegenerative disease that is characterized by degeneration of upper and lower

motor neurons (MN). This process leads to spasticity, muscle atrophy, and paralysis, which develop into respiratory failure and patient death (Frey *et al*, 2000; Fischer *et al*, 2004; Boillée *et al*, 2006; Moloney *et al*, 2014; Peters *et al*, 2015). The most common mutations responsible for familial ALS (fALS) include expansions of a repeated DNA element (GGGGCC) in the *C9orf72* gene and point mutations in the superoxide dismutase 1 (*SOD1*) gene (Rosen *et al*, 1993; DeJesus-Hernandez *et al*, 2011; Renton *et al*, 2011).

A hallmark finding in ALS patients, as well as in ALS mouse models, is alterations in axonal transport (Bilsland *et al*, 2010; Perlson *et al*, 2010; Gershoni-Emek *et al*, 2015; De Vos & Hafezparast, 2017). In order to survive and function, MNs depend upon the propagation of signaling events along the axons between the synapse and soma (cell body) (Harrington & Ginty, 2013; Millecamps & Julien, 2013; Terenzio *et al*, 2017; Zahavi *et al*, 2017). Retrograde and anterograde axonal transport are mediated by the dynein/dynein-actin and kinesin motor protein families, respectively (Paschal & Vallee, 1987; Howard *et al*, 1989; Guedes-Dias & Holzbaur, 2019). Notably, mutations in kinesin and dynein/dynein are also associated with ALS in humans (LaMonte *et al*, 2002; Münch *et al*, 2004; Steinberg *et al*, 2015; Nicolas *et al*, 2018). Several studies have suggested that alterations in cross-talk and long-distance signaling pathways between neurons and their diverse extracellular cues, which are mediated by axonal transport, contribute to ALS pathology (Boillée *et al*, 2006; Perlson *et al*, 2009; Gibbs *et al*, 2018).

Collapsin response mediator proteins (CRMPs) constitute a family of developmentally regulated phosphoproteins known for their intracellular mediation of class 3 semaphorin signaling (Goshima *et al*, 1995; Ziak *et al*, 2020). There are 5 known CRMPs in vertebrates, all of which share high sequence similarities (Schmidt & Strittmatter, 2007). The semaphorin/CRMP signaling pathway involves phosphorylation of CRMPs via various kinases including Rho-kinase, CDK5, or GSK3 β , which leads to microtubule destabilization and axon

1 Sackler Faculty of Medicine, Tel Aviv University, Tel Aviv, Israel

2 Sagol School of Neuroscience, Tel Aviv University, Tel Aviv, Israel

3 Institute of Physiology of the Czech Academy of Sciences, Prague, Czech Republic

4 Faculty of Science, Charles University, Prague, Czech Republic

5 Department of Neurology, University of Michigan, Ann Arbor, MI, USA

6 Department of Pathology, Sheba Medical Center, Tel Hashomer, Ramat Gan, Israel

7 The Mina and Everard Goodman Faculty of Life Science, Bar Ilan University, Israel

8 Department of Neurology, Sheba Medical Center, Tel Hashomer, Ramat Gan, Israel

*Corresponding author. Tel: +972-3-6408743; E-mail: eranpe@tauex.tau.ac.il

†These authors contributed equally to this work

retraction (Sasaki *et al*, 2002; Yamashita & Goshima, 2012; Balastik *et al*, 2015). In addition to their role in mediating semaphorin intrinsic cell responses, CRMPs have been reported to bind dynein and kinesin and modulate their function (Arimura *et al*, 2009; Rahajeng *et al*, 2010). Several studies have demonstrated the involvement of CRMPs in neurodegenerative diseases and neuronal injury (Charrier *et al*, 2003; Jang *et al*, 2010; Yamashita & Goshima, 2012; Nagai *et al*, 2017). Specifically, CRMP4 expression levels were found to be elevated in the SOD1^{G93A} mouse spinal cord and were suggested to promote MN death (Duplan *et al*, 2010; Valdez *et al*, 2012; Nagai *et al*, 2015). Interestingly, mutations in CRMP4 are associated with ALS (Blasco *et al*, 2013). However, the mechanism of CRMP4-mediated MN cell death in ALS is unknown.

Here, we identify a novel mechanism by which CRMP4 mediates MN toxicity in ALS. We discover a CRMP4-dependent retrograde signal in ALS that facilitates MN loss. This process is mediated by alterations of CRMP4 expression and the formation of a CRMP4-dynein complex via a specific motif in the CRMP4 protein in a subtype of ALS-diseased MN axons.

Results

Alterations in CRMP4 protein levels along ALS-diseased motor unit

Increased CRMP4 levels in MN cell bodies of the SOD1^{G93A} ALS mouse model were previously reported to be toxic to MNs and lead to cell death (Duplan *et al*, 2010). Specific mutations in the N-terminus of CRMP4 are associated with ALS in patients (Duplan *et al*, 2010; Valdez *et al*, 2012; Nagai *et al*, 2015). However, how CRMP4 mediates its toxicity in ALS MNs remains unknown. To address this, we first measured CRMP4 protein levels in the spinal cord of human ALS patients (Fig 1A and B). Consistent with the published results from the SOD1^{G93A} ALS mice model (Duplan *et al*, 2010), we observed a significant 2.5-fold increase in the relative CRMP4 expression in sALS patient compared to non-diseased controls (mean: healthy 1.285 ± 0.184 ; sALS patient 2.571 ± 0.137) (Fig 1A and B). This increase was also prevalent in SOD1^{G93A} mice spinal cord, as the total number of cells expressing CRMP4 in the

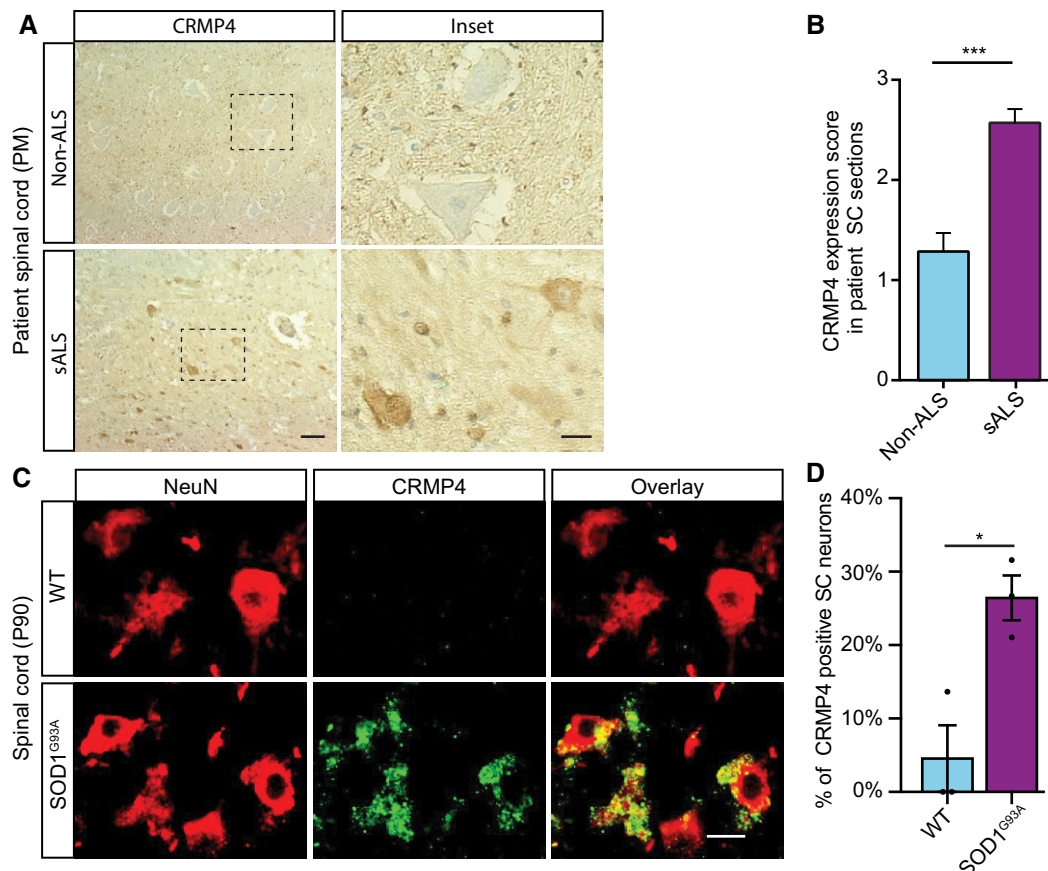


Figure 1. CRMP4 is elevated in ALS-diseased spinal cord neurons.

A, B (A) Representative IHC images and (B) semi quantification of CRMP4 protein in human spinal cords (SC) cross sections from 2 controls and 3 ALS patients. We analyzed total of 7 SC sections of controls and 14 SC sections of ALS patients, data presented as mean \pm SE. DAB: labeled CRMP4. Scale bar: left images 20 μ m, right insets 10 μ m. Mann-Whitney test *** P = 0.0003.
 C Representative images of P90 SC cross sections of SOD1^{G93A} and WT mice. Red: denotes NeuN, Green: denotes CRMP4. Scale bar: 10 μ m.
 D Quantification of the percentage of CRMP4-positive SC neurons in 3 WT VS. 3 SOD1^{G93A} mice. We monitored CRMP4 expression in total of 108 cells in WT condition and 123 cells in SOD1^{G93A}, an average of 36 or 41 cells in each repeat respectively. Student's t -test, n = 3, data presented as mean \pm SE, * P = 0.0161.

SOD1^{G93A} postnatal day 90 (P90) spinal cord compared to their littermate control was elevated (Fig 1C and D) (mean: WT 4.54 ± 4.4%; SOD1^{G93A} 26.43 ± 3.04%). Next, we determined the expression levels of CRMP4 in the distal parts of the motor neuron: (i) intra-muscular axons and (ii) neuromuscular junctions (NMJs). Unexpectedly, our analysis in human intra-muscular nerves from sALS patients, revealed a significant 28% decrease in CRMP4 levels within neurofilament heavy chain (NFH)-positive axons compared with healthy controls and a similar non-significant trend in MBP-positive Schwann cells (Fig 2 A,B) (Appendix Fig S1A and B) (mean intensity: non-ALS 1.00 ± 0.097; ALS 0.719 ± 0.108). Furthermore, analysis of P90 gastrocnemius muscles (GC) revealed a decrease in the number of NMJs expressing CRMP4 in SOD1^{G93A} mice compared to the WT control (Fig 2C and D) (the mean percentage of P90 NMJs expressing CRMP4: WT 90.6595 ± 4.78%; SOD1^{G93A} 60.29 ± 9.00%). Interestingly, we detected early partial NMJ degeneration in CRMP4-negative NMJs, suggesting an active role for CRMP4 in preservation of distal axons (Fig 2C and E) (the mean percentage of P90 partially innervated SOD1^{G93A} NMJs: CRMP4-positive 33.33 ± 16.67%; CRMP4-negative 91.67 ± 8.33%). Lastly, we monitored CRMP4 expression levels in WT and SOD1^{G93A} P90 sciatic nerves by immunostaining. We detected a 3-fold increase in CRMP4 signal in sciatic nerve axons (NFH-positive) and a moderate 70% increase in CRMP4 signal also in GFAP-positive cells in SOD1^{G93A} mice compared to the controls (Fig 2F and G; Appendix Fig S1C and D) (mean area: WT 1.00 ± 0.146; SOD1^{G93A} 2.817 ± 0.32) (mean area: WT 0.763 ± 0.127; SOD1^{G93A} 1.415 ± 0.25). Western blot analysis of SOD1^{G93A} and WT P90 sciatic axoplasm confirmed this overall increase in CRMP4 levels in ALS sciatic nerves (Fig 2H and I) (mean: WT 0.56 ± 0.11; SOD1^{G93A} 1.22 ± 0.14). Thus, our data thus far reveal that, while the expression levels of CRMP4 increase in cell bodies and proximal nerves, the opposite trend occurs in the distal/terminal parts of ALS-diseased MNs. This suggests that in ALS, distal-CRMP4 is mislocalized into proximal axons and cell bodies.

CRMP4 protein mislocalization via dynein-dependent activity

To investigate the potentially disease-relevant function of this intracellular mislocalization of CRMP4, we utilized human iPSC-derived

MNs (iPS-MN) from healthy controls and C9orf72-ALS patients (Tank *et al*, 2018) and plated them in microfluidic chambers (MFCs). First, we immunostained for the neuronal/axonal markers NFH and Tau, along with the MN-specific marker HB9, to validate the MN cell identity (Appendix Fig S2A–F). Then, we performed immunostaining for CRMP4 to assess changes in its levels in distal axons (Fig 3A–D). Our analysis revealed no difference in CRMP4 intensity levels between healthy and C9orf72 iPS-MN axons in this system (Fig 3A and B). In our previous study, we demonstrated that muscle-secreted *Sema3A* leads to NMJ's disruption and axonal degeneration in ALS (Maimon *et al*, 2018). The canonical pathway for CRMP activation involves *Sema3A*-NRP-PlexinA interactions. Therefore, we considered whether CRMP4 requires stress activation for differential, disease-relevant mislocalization in MNs cultures and asked whether *Sema3A* treatment might differentially affect CRMP4 levels in ALS iPS-MNs versus Healthy iPS-MNs. We found that exposing distal axons to *Sema3A* for 8 h led to significant increase in CRMP4 intensity specifically in axons of C9orf72 MNs (mean: healthy 0.7 ± 0.05; Healthy + *Sema3A* 0.75 ± 0.047; C9orf72 0.61 ± 0.03; C9orf72 + *Sema3A* 1.27 ± 0.16) (Fig 3A and B). Given that CRMP4 levels were specifically high in somata and proximal axons of ALS patients and SOD1^{G93A} mice, we tested the CRMP4 levels in somata and proximal axons of C9orf72 and healthy iPSC-MNs following distal *Sema3A* treatment. We used cholera toxin B-647 (CTX) retrograde tracing to specifically examine CRMP4 levels in proximal axons and somata parts of neurons that send their axons into distal compartment of MFC (Fig 3C). Looking specifically at this neuronal population, we detected an increase in CRMP4 intensity post *Sema3A* treatment in C9orf72 iPS-MN soma and proximal axons but not in healthy iPS-MN controls (Fig 3D–G) (CRMP4 mean intensity in somata area, measured by GAPDH outline: healthy 1.00 ± 0.128; Healthy + *Sema3A* 1.222 ± 0.148; C9orf72 1.00 ± 0.078; C9orf72 + *Sema3A* 1.258 ± 0.068) (CRMP4 mean intensity proximal axons: Healthy 1.00 ± 0.066; Healthy + *Sema3A* 1.048 ± 0.059; C9orf72 1.00 ± 0.093; C9orf72 + *Sema3A* 1.302 ± 0.11).

CRMPs have been reported to bind to the dynein motor protein and modulate its function (Arimura *et al*, 2009; Rahajeng *et al*, 2010). Since distal exposure to *Sema3A* led to CRMP4 elevation in the ALS-diseased MN soma, we speculated that CRMP4 undergoes

Figure 2. CRMP4 is mislocalized in ALS motor units.

- A Representative images of ALS patient or non-ALS human control intra-muscular nerves. Red: denotes NFH, Green: denotes CRMP4, White: denotes co-localization area using Imaris software. Scale bar: 20 μm.
- B Quantification of CRMP4 intensity levels in NFH-positive intra-muscular distal nerves from 5 non-ALS controls and 4 sALS patients. We analyzed 40 terminal axons from the healthy samples (~ 8 axons per sample) and 36 terminal axons from sALS samples (~ 8 axons per sample). Data presented as mean ± SE. Student's *t*-test, **P* = 0.0475.
- C Representative images of SOD1^{G93A}/ChAT::tdTomato or WT^{ChAT::tdTomato} neuromuscular junctions (NMJ's) at P90. White: denotes BTX, Red: denotes direct ChAT, Green: denotes CRMP4, Yellow: denotes Z projection of 3D Imaris co-localization of CRMP4 and ChAT. Scale bar: 10 μm.
- D Quantification of CRMP4-positive NMJ's in gastrocnemius muscles from 3 WT or 3 SOD1^{G93A} P90 mice. Total of 44 NMJ's in WT condition and 60 NMJ's in SOD1^{G93A} condition. Student's *t*-test, *n* = 3, data presented as mean ± SE, **P* = 0.0157.
- E Quantification of the percent of partially denervated NMJ's in the presence or absence of CRMP4 immunostaining in 3 different SOD1^{G93A} mice. We counted 24 NMJ's in SOD1^{G93A} CRMP4 negatives and 67 NMJ's in SOD1^{G93A} CRMP4 positives. Student's *t*-test, *n* = 3, data presented as mean ± SE, **P* = 0.0352.
- F Representative images of P90 SOD1^{G93A} and WT sciatic nerves. Red: denotes NFH, Cyan: denotes GFAP and green denotes CRMP4, Yellow: denotes the Z projection of 3D Imaris co-localization of CRMP4 and NFH. Scale bar: 5 μm.
- G Quantification of the co-localization area of CRMP4 with NFH in the sciatic nerve in 3 SOD1^{G93A} mice compared to 3 WT mice using Imaris analysis. 14 WT sciatic nerve sections and 11 SOD1^{G93A} sections were monitored. Data presented as mean ± SE. Student's *t*-test, *n* = 3, *****P* < 0.0001.
- H, I Western blot analysis and quantification of 3 independent repeats of P90 SN tissues for CRMP4 expression levels (size of ~ 64 kDa) in SOD1^{G93A} compared to WT. tERK was used as a loading control (size of ~ 44 kDa). Student's *t*-test, *n* = 3, data presented as mean ± SE, **P* = 0.0215.

Source data are available online for this figure.

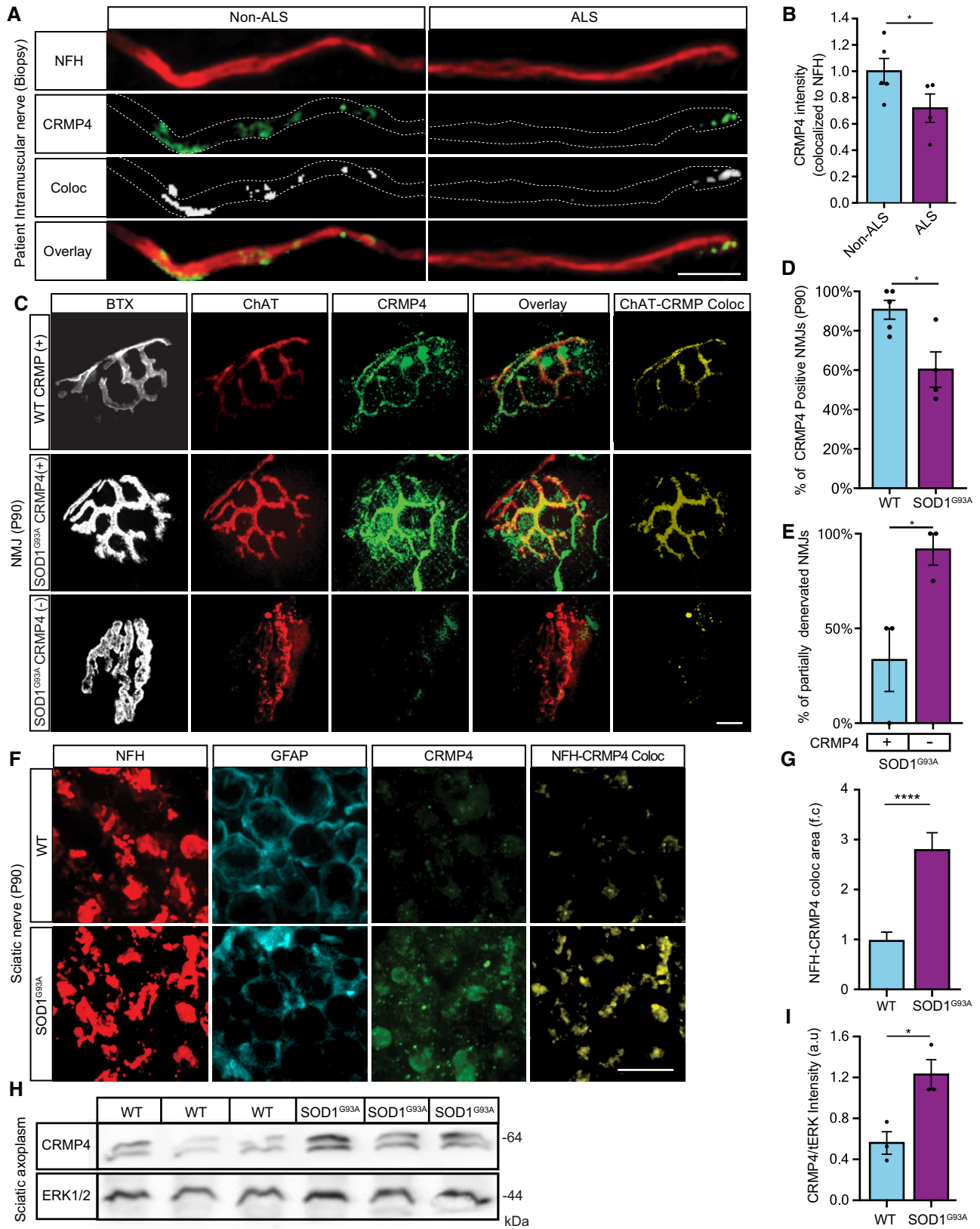


Figure 2.

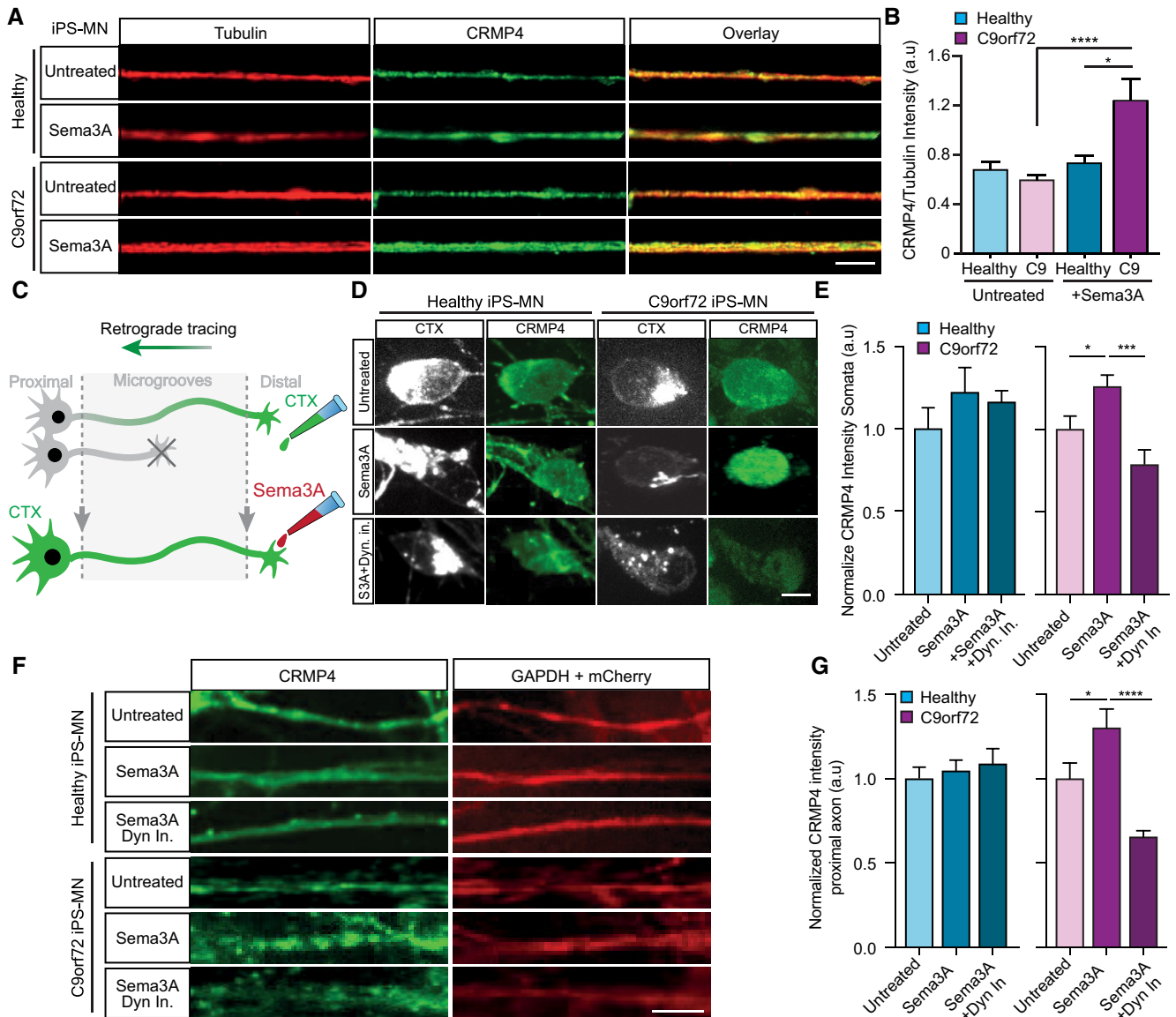


Figure 3. CRMP4 protein levels are altered via a dynein-dependent activity.

A Representative images of healthy or *C9orf72* iPSC-derived MNs treated with Sema3A or untreated in the distal compartment, 8 h post-treatment. Red: denotes Tubulin, Green: denotes CRMP4. Scale bar: 5 μ m.

B Quantification of CRMP4 intensity levels in healthy or *C9orf72* iPSC-derived MNs with Sema3A treatment or untreated. 14 untreated healthy axons, 12 healthy axons with Sema3A treatment, 49 untreated *C9orf72* axons, and 31 *C9orf72* axons with Sema3A treatment were monitored from 3 different chambers. One-way ANOVA, Tukey's multiple comparisons test, $n = 3$, data presented as mean \pm SE, $*P = 0.0338$; $****P < 0.0001$.

C Illustration of the experimental procedure for MNs in an MFC treated with the fluorescently tagged retrograde tracer CTX in the distal compartment. Neuronal cell bodies in the primary neuron whose axons have traversed into the distal compartment were also labeled by the retrograde tracer.

D Representative images of healthy or *C9orf72* human-derived MN cell somata with Sema3A treatment, Sema3A + dynein inhibitor treatment, or untreated. Gray: denotes CTX, Green: denotes CRMP4. Scale bar: 5 μ m.

E Quantification of CRMP4 intensity (normalized to GAPDH + mCherry/area) levels at the somata of healthy or *C9orf72* human-derived MN after Sema3A treatment, Sema3A + dynein inhibitor treatment, or untreated. Analysis performed in 3 independent chambers per condition. 19 healthy untreated cell somata, 26 healthy cell somata with Sema3A treatment, 20 healthy cell somata with Sema3A + dynein inhibitor treatment and 14 *C9orf72* cell somata from each condition were monitored. One-way ANOVA, Newman-Keuls multiple comparisons test, $n = 3$, data presented as mean \pm SE, $*P = 0.0207$; $***P = 0.0004$.

F Representative images of healthy or *C9orf72* human-derived MN proximal axons with Sema3A treatment, Sema3A + dynein inhibitor treatment, or untreated control. Green: denotes CRMP4, Red: denotes GAPDH. Scale bar: 5 μ m.

G Quantification of CRMP4 intensity levels (normalized to GAPDH + mCherry/area) at the proximal axons in healthy or *C9orf72* human-derived MN after Sema3A treatment, Sema3A + dynein inhibitor treatment, or untreated control. Analysis performed from 3 independent chambers in each condition. 21 healthy untreated proximal axons, 24 healthy proximal axons with Sema3A treatment, 16 healthy proximal axons with Sema3A + dynein inhibitor treatment, 12 *C9orf72* untreated proximal axons, 8 *C9orf72* proximal axons with Sema3A treatment and 13 *C9orf72* proximal axons with Sema3A + dynein inhibitor treatment were monitored. One-way ANOVA, Newman-Keuls multiple comparisons test, $n = 3$, data presented as mean \pm SE, $*P = 0.0334$, $****P < 0.0001$.

retrograde transport mediated by dynein. Therefore, we examined CRMP4 levels in the cell bodies and proximal axons of healthy and C9orf72 iPS-MNs that were distally exposed to Semaphorin 3A with or without the presence of the dynein inhibitor, Ciliobrevin D (herein Dyn-In) (Firestone *et al*, 2012) (Fig 3D–G). Inhibiting dynein completely blocked Semaphorin 3A-induced increase in CRMP4 levels in C9orf72 iPS-MNs axons and somata (Fig 3D–G; Appendix Fig S3A and B) (CRMP4 mean intensity somata—measured by GAPDH outline: Healthy + Semaphorin 3A 1.222 ± 0.148 ; Healthy + Semaphorin 3A + Dyn in 1.161 ± 0.067 ; C9orf72 + Semaphorin 3A 1.258 ± 0.068 ; C9orf72 + Semaphorin 3A + Dyn in 0.787 ± 0.088) (CRMP4 mean intensity proximal axons: Healthy + Semaphorin 3A 1.048 ± 0.059 ; Healthy + Semaphorin 3A + Dyn in 1.087 ± 0.089 ; C9orf72 + Semaphorin 3A 1.302 ± 0.11 ; C9orf72 + Semaphorin 3A + Dyn in 0.655 ± 0.036). We did not observe this effect in the presence of Dyn-In alone (Appendix Fig S3A and B). Furthermore, to validate that distal Semaphorin 3A treatment has effect on MN soma, we quantified the cell body area (by measuring CTX signal outline) and found that C9orf72 Semaphorin 3A-treated MNs exhibit smaller soma areas compared to untreated or healthy MNs cultures (Appendix Fig S3C). Here again, when dynein activity was inhibited prior to Semaphorin 3A application, this effect abolished (mean area: Healthy untreated 302 ± 29 ; Healthy + Semaphorin 3A 285 ± 15 ; Healthy + Semaphorin 3A + Dyn-In 296 ± 18 ; C9orf72 untreated 314 ± 10 ; C9orf72 + Semaphorin 3A 263 ± 10 ; C9orf72 + Semaphorin 3A + Dyn-In 318 ± 12) (Appendix Fig S3C). Importantly, no differences were monitored post-application of Dyn-In alone in both healthy and disease conditions. These data indicate that the elevation in CRMP4 in cell bodies and in proximal axons of ALS-diseased neurons is mediated by dynein, likely by binding to axonal CRMP4 and subsequent retrograde transport to the cell body.

A specific CRMP4 motif mediates the CRMP4-dynein-dynactin interaction

CRMP2 members were previously found to bind the dynein motor protein (Arimura *et al*, 2009). Arimura *et al* (2009) also characterized two specific domains in the CRMP2 protein that are responsible for dynein binding (Arimura *et al*, 2009). Since CRMP2 and CRMP4 share substantial sequence similarity, we hypothesized that the dynein-binding domains (100aa–150aa) of CRMP2 would play a similar role in CRMP4. Following this, and on the basis of the CRMP4 protein 3D structure (PDB code 4CNT) (Ponnusamy *et al*, 2014) (Fig 4A), we overexpressed full-length GFP-CRMP4 or CRMP4 lacking amino acids 100–150 (GFP-CRMP4 Δ 100–150) in COS7 cells and immunoprecipitated the endogenous dynein intermediate chain (DIC). Western blot analysis of these fractions revealed a clear interaction of DIC with full-length GFP-CRMP4 but not with GFP-CRMP4 Δ 100–150 (Fig 4B) (mean: GFP-CRMP4 1.473 ± 0.373 ; GFP-CRMP4 Δ 100–150 0.009 ± 0.001). Since a large deletion in the CRMP4 protein sequence may result in its misfolding and dysfunction, we pursued an alternative strategy by generating small peptides to cover the potential dynein-binding motif and test whether this could block dynein binding to CRMP4. We designed four short peptides within the 50 amino acid domain, which exhibit the potential to block CRMP4-dynein interaction, based on the protein structure. Importantly, the peptide sequences were designed to avoid an overlap with CRMP4 homo-tetramer interfaces, likely preventing a disturbance to the protein's homomeric assembly

(Fig 4A). To test the peptide activity, we pre-incubated a mixture of peptides 1–4 with lysate from GFP-CRMP4 overexpressing COS7 cells. This process significantly reduced the CRMP4-DIC interaction (Fig 4B and C; mean: GFP-CRMP4 1.473 ± 0.373 ; GFP-CRMP4 + peptides 0.3 ± 0.05). We also examined CRMP4 interaction with dynactin (p150), a dynein activator, in COS7 cells overexpressing Flag-tagged CRMP4. After an overnight incubation of cell lysate with peptides 1–4, we pulled down Flag-CRMP4 and blotted for dynactin (p150). Application of the peptide mixture resulted in a dramatic decrease in CRMP4 binding to dynactin (Fig 4D and E) (mean: control 0.77 ± 0.1 ; All peptides 0.17 ± 0.06). We also determined whether introducing the individual peptides might be sufficient to also block the CRMP4-dynactin interaction. Using the same assay, we incubated each peptide separately and found that only peptide-4 had a mild but significant ability to block CRMP4 interaction with dynactin (Fig 4F and G) (mean: control 1.92 ± 0.2 ; peptide-1 1.44 ± 0.3 ; peptide-2 1.34 ± 0.3 ; peptide-3 1.8 ± 0.8 ; peptide-4 1.13 ± 0.14). Hence, although peptide-4 was sufficient to block CRMP4-dynactin binding, blocking CRMP4-dynactin complex formation requires a combination of all four peptides. Lastly, we generated a genetic tool to block the CRMP4-dynein interaction using a plasmid with CRMP4-dynein-binding motif sequence (corresponding to a.a 100–150 of CRMP4) and determined whether it could act in a dominant-negative manner. We transfected COS7 cells with GFP or GFP-expressing 50aa sequence (GFP-50aa) and then extracted the cells and assayed for CRMP4 that co-purified with the dynein intermediate chain (DIC) via immunoprecipitation. Our Western blot analysis revealed weaker interaction of CRMP4 with dynein in the presence of GFP-50aa overexpressing cells compare to the control (mean: GFP-CRMP4 1.00 ± 0.10 ; GFP-50aa 0.54 ± 0.11) (Fig 4H and I). Thus, amino acids 100–150 in the CRMP4 protein are essential for CRMP4/dynein/dynactin binding.

Enhanced CRMP4-dynein complex formation in ALS-diseased MNs

Our data thus far suggest that CRMP4 levels are (i) increased in the cell soma and (ii) decreased in the NMJs and distal axons of ALS-diseased MNs (Figs 1 and 2). We further demonstrate that CRMP4 mislocalization in ALS-diseased MNs can be facilitated by Semaphorin 3A and is mediated by dynein (Figs 3 and 4). Since our previous report suggests elevations in Semaphorin 3A secretion from ALS muscles (Maimon *et al*, 2018), we predicted an increase in CRMP4-dynein complex formation along the axons of ALS models. To test this, we first extracted sciatic nerves axoplasm from WT and SOD1^{G93A} P90 mice and measured the levels of CRMP4 that co-purified with the dynein intermediate chain (DIC) *in vivo* using immunoprecipitation. We found a stronger interaction of DIC with CRMP4 in the SOD1^{G93A} mice compared with the control (Fig 5A and B) (mean: WT 0.28 ± 0.11 ; SOD1^{G93A} 1.48 ± 0.62). Notably, transfecting cells with CRMP4 that carries an ALS-associated mutation, I141V, also enhanced the formation of the CRMP4-dynein complex (Fig 5C and D) (mean: WT CRMP4 1.00 ± 0.207 ; mutated CRMP4 1.625 ± 0.116). Importantly, I141V is located in the same dynein-binding motif in the CRMP4 protein, suggesting a CRMP4 gain of toxic function in ALS.

To further characterize CRMP4-dynein interactions in ALS, we attempted to track CRMP4-GFP retrograde movement in healthy and

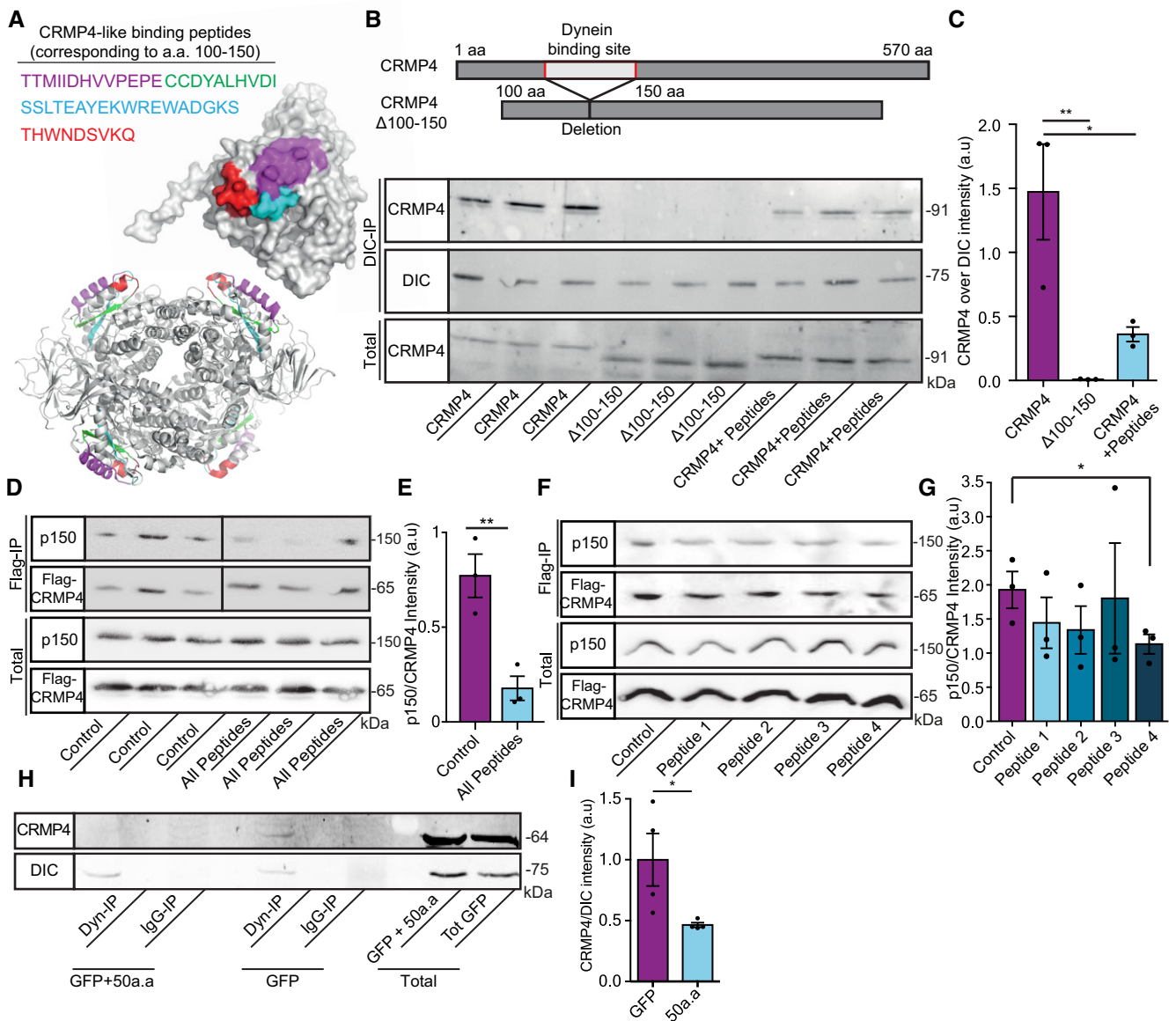


Figure 4. CRMP4 binds dynein via a specific 50 amino acid motif.

- A Crystal structures (PDB code 4CNT) of a CRMP4 monomer (upper panel) and biological tetramer assembly (lower panel). The peptides that were selected to inhibit binding are highlighted and color coded as indicated.
- B Upper panel represents the binding site domain of dynein in CRMP4 and its deletion. Middle panel—Immunoprecipitation of DIC followed by western blot analysis of CRMP4 in COS7 cells overexpressing either GFP-CRMP4, or GFP-CRMP4 with deletion of amino acid 100–150, or GFP-CRMP4 overexpressing cells that were pre-incubated with a 10 μ m mixture of peptides 1–4 (size of ~ 91 kDa). Lower panel - Western blot analysis of total protein levels before the pull-down assay (DIC size: ~ 75 kDa).
- C Quantification of the Western blot in B from 3 independent repeats. One-way ANOVA, Tukey's multiple comparisons test, $n = 3$, data presented as mean \pm SE, $**P = 0.007$, $*P = 0.0261$.
- D Upper panel - immunoprecipitation assay with anti-Flag antibody followed by Western blot analysis of dynactin (p150) (size of ~ 150 kDa) in COS7 cells overexpressing Flag-CRMP4 (size of ~ 65 kDa). Lower panel - total protein input.
- E Quantification of the blot in D from 3 independent repeats. The dynactin intensity band was normalized to the Flag-CRMP4 intensity band in each repeat. Student's t -test, $n = 3$, data presented as mean \pm SE, $**P = 0.01$.
- F Upper panel - Immunoprecipitation assay with anti-Flag antibody followed by Western blot analysis of dynactin (p150) (size of ~ 150 kDa) in COS7 cells overexpressing Flag-CRMP4 (size of ~ 65 kDa). Lower panel - Total input.
- G Quantification of the blot in F. The dynactin intensity band was normalized to the Flag-CRMP4 intensity band in each repeat. Student's t -test, $n = 3$, data presented as mean \pm SE, $*P = 0.0299$.
- H Immunoprecipitation of DIC (size of ~ 75 kDa) followed by Western blot analysis of CRMP4 (size of ~ 64 kDa) in COS7 cells that were transfected with CRMP4 and AAV9-50aa or its control. IgG antibody was used as a control.
- I Quantification of the blot in H from 3 independent repeats. The CRMP4 intensity band was normalized to the DIC intensity band in each repeat. Student's t -test, $n = 3$, data presented as mean \pm SE, $*P = 0.0479$.

Source data are available online for this figure.

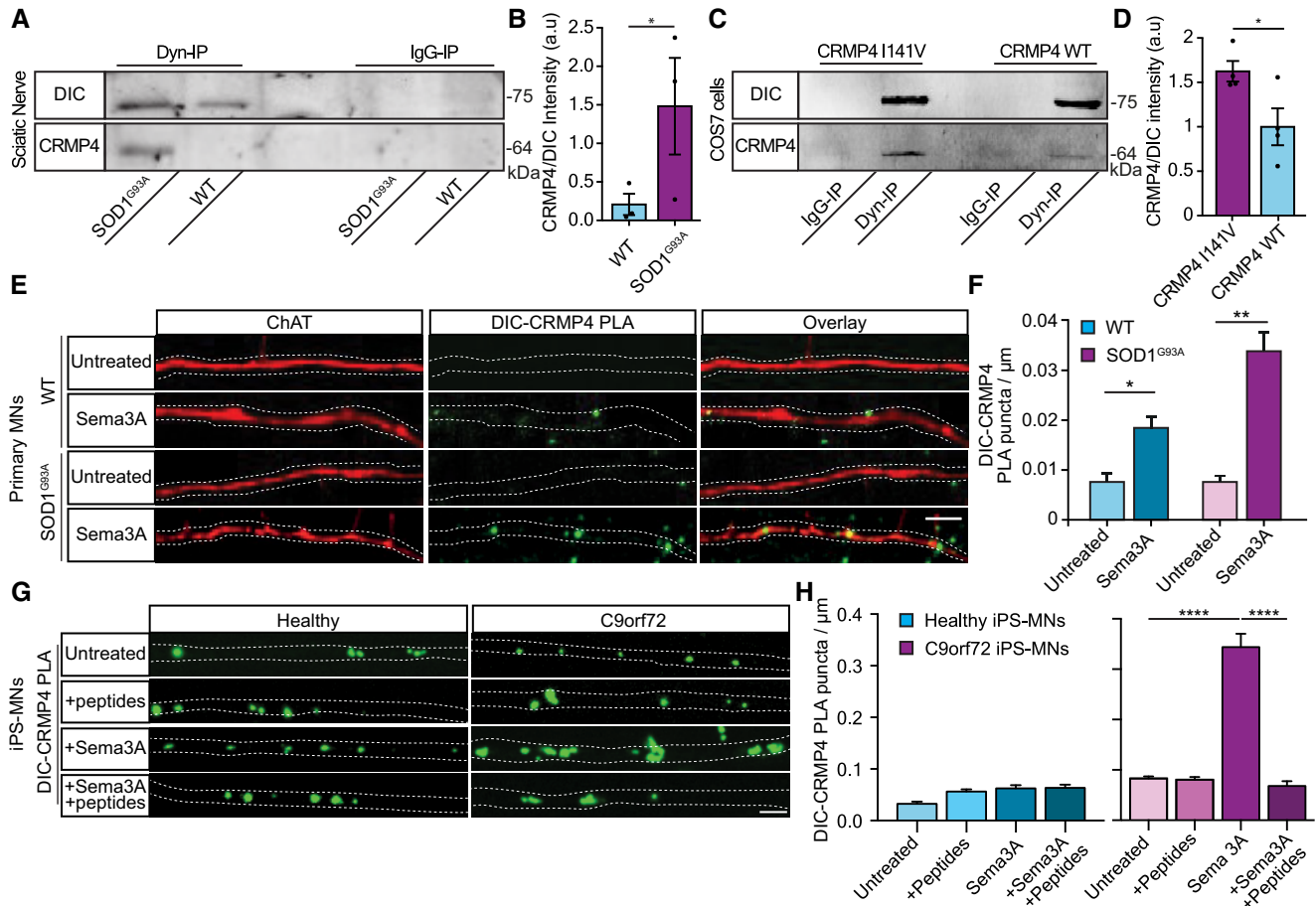


Figure 5. CRMP4-dynein interaction is enhanced in ALS motor neuron axons.

A Immunoprecipitation of DIC followed by Western blot analysis of CRMP4 in SOD1^{G93A} compared to WT P90 sciatic nerves under physiological conditions. IgG antibody was used as a control.

B Quantification of the blot in A. 3 repeats, 12 sciatic nerves per condition were used in each repeat. The CRMP4 intensity band was normalized to the DIC intensity band in each repeat. Data presented as mean ± SE (Ratio Paired t-test, *P = 0.0416).

C Immunoprecipitation of DIC followed by Western blot analysis of CRMP4 in COS7 cells that were transfected with mutant CRMP4 I141V compared to control. IgG antibody was used as a control.

D Quantification of four repeated pull down in C. The CRMP4 intensity band was normalized to the DIC intensity band for each repeat. (Student's t-test, n = 4, data presented as mean ± SE, *P = 0.0393).

E Representative images from the proximity ligation assay (For explanation of PLA technique; please refer to method section) for CRMP4 and dynein in SOD1^{G93A} and WT primary MNs axons that were exposed to either control or Sema3A 8h post-treatment. Scale bar: 5µm.

F Quantification of the CRMP4-DIC puncta number per primary motor neuron axon in each condition. We analyzed ~ 20 axons per condition from 3 independent chambers per group (One-way ANOVA, Tukey's multiple comparisons test, n = 3, data presented as mean ± SE, **P = 0.01, *P = 0.04).

G Representative images of proximity ligation assay for CRMP4 and dynein in healthy and C9orf72 human-derived proximal axons post peptides treatment, Sema3A treatment, Sema3A + peptides treatment, or untreated controls. Scale bar: 5 µm.

H Quantification of the CRMP4-DIC puncta number per axon in healthy or C9orf72 human-derived MN proximal axons after Sema3A treatment, Sema3A + peptides treatment, or untreated controls. Data collected from 3 independent chambers in each condition. Total of 37 healthy untreated proximal axons, 61 healthy proximal axons with peptides treatment, 59 healthy proximal axons with Sema3A treatment and 52 healthy proximal axons with Sema3A + peptides treatment. 67 C9orf72 untreated proximal axons, 63 C9orf72 proximal axons with peptides treatment, 41 C9orf72 proximal axons with Sema3A treatment, and 50 C9orf72 proximal axons with Sema3A + peptides treatment monitored. Data presented as mean ± SE. One-way ANOVA, Tukey's multiple comparisons test, n = 3, ****P < 0.0001.

Source data are available online for this figure.

ALS-diseased MN axons. However, overexpressing CRMP4-GFP resulted in a uniformly diffuse distribution (Appendix Fig S4). Thus, in order to demonstrate retrograde transport of endogenous CRMP4, we immunostained distinct cellular compartments (dynein and CRMP4) using proximity ligation assay (PLA), as previously performed (Olenick *et al*, 2019). First, by using PLA, we observed that indeed there is an increase in the CRMP4-dynein co-localization

along cultured WT MNs axons, post-Sema3A treatment compared to untreated WT cultures (Fig 5E). Importantly, this co-localization was twice as high in the Sema3A-treated SOD1^{G93A} MNs axons (Fig 5E and F). Furthermore, when comparing co-localization patterns of the CRMP4-dynein puncta in human iPS-MNs in the presence or absence of Sema3A, we obtained similar results: In naive, untreated axons, the number of CRMP4-dynein puncta was

similar between healthy and C9orf72 iPS-MNs. However, following Semaphorin 3A (Sema3A) treatment, the number of CRMP4-dynein puncta in C9orf72 axons was significantly higher compared to treated healthy control (Fig 5G and H) (mean puncta per axon: healthy untreated 0.032 ± 0.004 ; Healthy + Sema3A 0.062 ± 0.006 ; C9orf72 untreated 0.082 ± 0.004 ; C9orf72 + Sema3A 0.344 ± 0.026). Next, in order to determine whether the formation of CRMP4-dynein complexes in MN axons is reversible, we aimed to block the CRMP4-dynein interaction in iPS-MN distal axons. To this end, we plated healthy and C9orf72 iPS-MNs in MFCs and exclusively introduced a mix of all peptides (1–4) into axons in the distal compartment. Using TAMRA peptides as a positive control for uptake, we observed that peptides 1–4 were successfully taken up by distal axons (Appendix Fig S5A and B). Strikingly, application of peptides 1–4 significantly interfered with the interaction of CRMP4 and dynein in distal C9orf72 iPS-MN axons as determined by PLA. CRMP4-dynein interaction in healthy iPS-MN remained unaffected by either Sema3A, peptides 1–4, or by both (Fig 5G and H) (mean puncta per axon: Healthy + Sema3A 0.062 ± 0.006 ; Healthy + Sema3A + peptide 0.063 ± 0.006 ; C9orf72 + Sema3A 0.344 ± 0.026 ; C9orf72 + Sema3A + peptide 0.067 ± 0.009). No differences were monitored when peptides were inserted without Sema3A activation in both conditions (Fig 5G and H) (mean puncta per axon: healthy untreated 0.032 ± 0.004 ; Healthy + peptides 0.056 ± 0.004 ; C9orf72 untreated 0.082 ± 0.004 ; C9orf72 + peptides 0.080 ± 0.005). Together, we have demonstrated both *in vivo* and *in vitro* that the CRMP4-dynein interaction is elevated in ALS-mutated MN axons. Importantly, this strong interaction can be blocked in ALS MN axons by interfering with the CRMP4-dynein-binding domain using both genetic and pharmacological tools.

The CRMP4-dynein complex facilitates selective neuronal loss in ALS

MNs undergo apoptosis and degenerate in ALS (Reyes et al, 2010). Downregulation of CRMP4 was previously suggested to inhibit neurodegeneration *in vitro* and *in vivo* in ALS models (Charrier et al, 2003; Duplan et al, 2010). Thus, we examined whether enhancement of the CRMP4-dynein interaction by Sema3A would lead to neuronal cell death in ALS. Similar to the experimental design in Fig 3C, we applied CTX to the distal compartment of the MFCs in order to label only the cell bodies of neurons whose axons traversed into the distal compartment. The number of CTX⁺ iPS-MNs was quantified before and 2 days after Sema3A was applied to the distal compartment. Our analysis did not detect any significant loss of CTX⁺ cells in healthy iPS-MNs in response to Sema3A, whereas in C9orf72 iPS-MNs we detected a ~ 25 percent decrease in CTX⁺ MNs upon treatment with Sema3A (Fig 6A–C). Similarly, applying Sema3A to spinal cord cultures from SOD1^{G93A} embryos resulted in a ~ 30% reduction in CTX⁺ MNs 3 days after treatment, compared with ~ 5% in the control and WT explants (Fig 6D and E; Appendix Fig S6) (mean fold change over control: Sema3A 0.68 ± 0.06 ; control 1 ± 0.04). In order to determine whether distal stress such as Sema3A application triggers MN loss in ALS-diseased MNs via retrograde signaling, we used dynein inhibitor to block all retrograde transport events (Firestone et al, 2012). Inhibiting retrograde transport in the distal axon prevented MN loss in the SOD1^{G93A} primary cultures (Fig 6D and E; Appendix Fig S6A–E)

(mean fold change over control: Sema3A + Dyn-In 0.92 ± 0.09 ; control 1 ± 0.04). Sema3A was previously shown to internalize together with its receptor, Plexin A1 (PLXNA1) in a dynamin-dependent manner (Fournier et al, 2000; Castellani et al, 2004). To further determine whether endocytosis of Sema3A is important for the apparent retrograde death signal, as shown before in different neurons (Wehner et al, 2016), we applied Dynasore, a dynamin-dependent endocytosis inhibitor (Macia et al, 2006), to the distal axons prior to application of Sema3A. Inhibiting Sema3A + PLXNA1 (Appendix Fig S7) internalization did not inhibit the loss of SOD1^{G93A} CTX⁺ MNs (Fig 6E; Appendix Fig S6) (mean fold change over control: Sema3A + Dynasore 0.71 ± 0.01 ; control 1 ± 0.04). Thus, Sema3A internalization at the distal axons is not required for the observed toxicity. Importantly, interfering with the CRMP4-dynein interaction by introducing peptides 1–4 into diseased iPS-MN axons prior to applying Sema3A completely abolished the CTX⁺ signal loss (mean: control 0.97 ± 0.009 ; Sema3A 0.813 ± 0.036 ; Sema3A + Pep 0.94 ± 0.019) (Fig 6F and G). Our findings demonstrate that death of ALS MNs following Sema3A application can be prevented by inhibiting the formation of CRMP4-dynein complexes.

We further examined whether impairing the CRMP4-dynein interaction *in vivo* reduces MN death, which is a hallmark in the SOD1^{G93A} mouse model. To this end, we chose to prevent CRMP4-dynein interaction using intrathecal injections of AAV9 viruses to insert CRMP4-dominant-negative construct (Fig 4H and I) into spinal cord MNs. First, to demonstrate injection efficacy, we immunostained spinal cord and sciatic nerve tissues that were infected with a control AAV9-GFP, by intrathecal injections (Appendix Fig S8A) and monitored the percentage of infected neurons by analyzing co-localization of the neuronal markers NeuN or NFH with GFP in spinal cords and axons along the sciatic nerves (Appendix Fig S8B and D). We found that 65% of spinal cord neurons as well as 50% sciatic nerve axons expressed GFP signal in AAV9-GFP injected mice compared to non-injected control (Appendix Fig S8C and D) (infected SC mean: non-injected $0.25 \pm 0.19\%$; AAV9-GFP $70.31 \pm 0.97\%$; infected SN mean: non-injected $0.25 \pm 0.163\%$; AAV9-GFP $53.98 \pm 4.233\%$). We then delivered AAV9-GFP-50aa/AAV9-GFP as a dominant-negative approach, into pre-symptomatic ~ P60 SOD1^{G93A} CSF by lumbar intrathecal injection and monitored for the activation of the apoptotic marker caspase 3 (Pasinelli et al, 1998; Porter, 1999; Reyes et al, 2010) 4 weeks post-injection (Fig 7A–E). Importantly, GFP signal was detected in similar number of spinal cord neurons and in similar intensity in both AAV treatments, meaning no difference in infection effectiveness between the GFP and GFP-50aa constructs (Appendix Fig S8E and F) (infected cells mean: AAV9-GFP $70.31 \pm 4.024\%$; 50aa-AAV9-GFP $76.38 \pm 2.965\%$) (GFP intensity mean: AAV9-GFP $3,955 \pm 318$; 50aa-AAV9-GFP $3,625 \pm 383$). We measured the degree of activated caspase 3 in P90 SOD1^{G93A} and compared it to the age-matched control. As expected, ~ 90% of NeuN-positive cells with MN morphology in the ventral horn were positive for activated caspase 3 in the spinal cord of SOD1^{G93A} mice, while only few caspase 3-positive neurons were detected in the control mice (Fig 7A and B) (mean: WT 12.18 ± 5.666 ; SOD1^{G93A} 92.67 ± 3.167). Injection with AAV9-GFP-50aa resulted in a ~ 25% decrease in the percentage of activated caspase

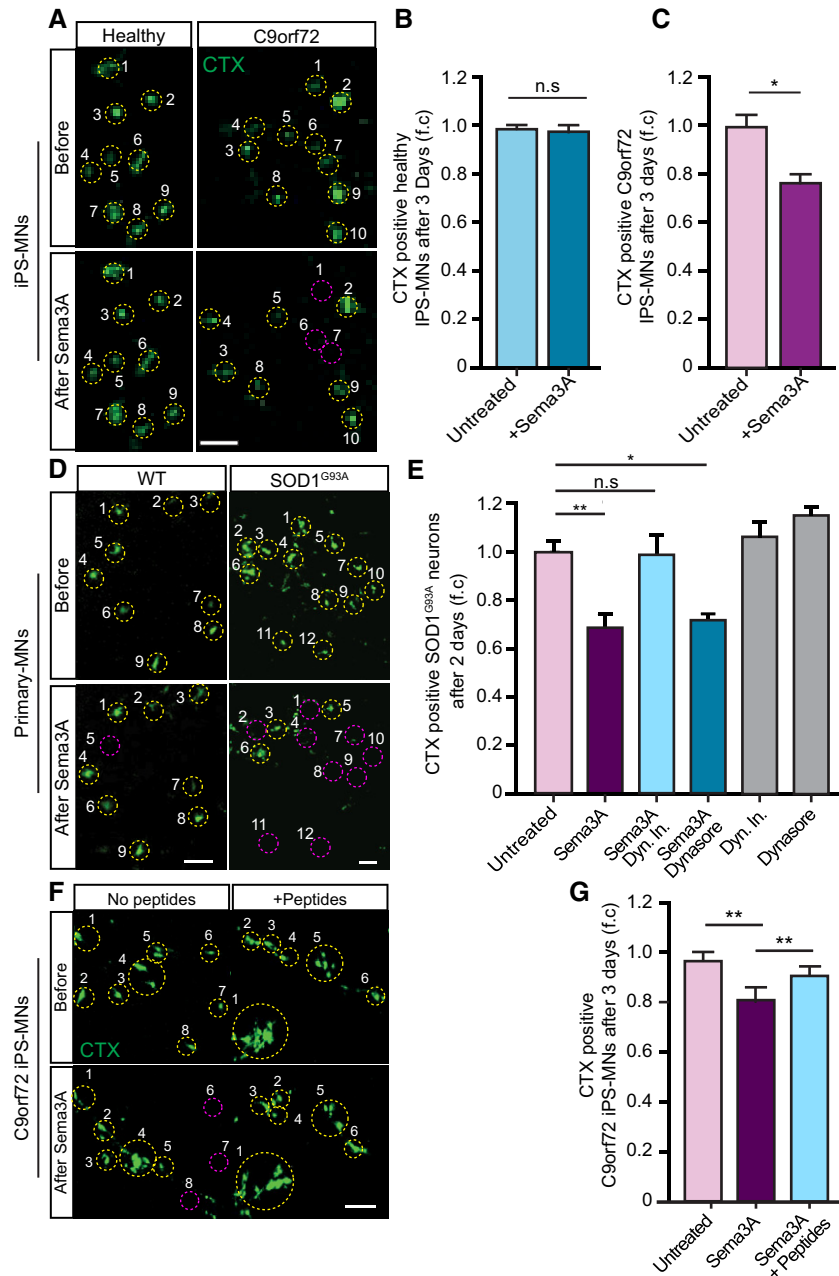


Figure 6. Retrograde CRMP4-dynein complex formation mediates MN loss in ALS.

- A** Representative images of CTX signal in healthy and C9orf72 human iPSC-derived MNs before and after Sema3A application. Green: denotes CTX-positive cells. Yellow circles are numbered CTX-positive cells. Purple circles are cells that are missing post Sema3A treatment. Scale bar: 40 μ m.
- B, C** Quantification of CTX signal in healthy and C9orf72 iPSC-derived MNs before and 3 days after applying Sema3A to distal compartment, compared with untreated control. 3 independent chambers in each condition were analyzed. Average of ~ 150 neurons per condition monitored. Student's *t*-test, $n = 3$, data presented as mean \pm SE, * $P < 0.05$.
- D** Representative images of CTX signal in WT or SOD1^{G93A} primary MNs before and 2 days after Sema3A application to the distal compartment in the presence of either Dynein inhibitor + Sema3A, Dynasore + Sema3A, or untreated. Green: denotes CTX-positive cells. Yellow circles are numbered CTX-positive cells. Purple circles are cells that are missing post Sema3A treatment. Scale bar: 30 μ m.
- E** Quantification of CTX signal in a SOD1^{G93A} explant before and 2 days after Sema3A application to the distal compartment in the presence of either Dynein inhibitor + Sema3A, Dynasore + Sema3A. 3 independent chambers in each condition were analyzed. ~ 200 neurons were monitored per each condition. One-way ANOVA, Tukey's multiple comparisons test, $n = 3$, data presented as mean \pm SE, * $P < 0.05$, ** $P < 0.01$. Dynein inhibitor and Dynasore treatments were used as a negative control.
- F, G** Representative images and quantification of C9orf72 iPSC-derived MNs in the proximal compartment of an MFC before and after Sema3A treatment with and without 10 μ g peptides 1–4. Green: denotes CTX-positive cells. Yellow circles are numbered CTX-positive cells. Purple circles are cells that are missing post Sema3A treatment. 3 independent chambers in each condition were analyzed. ~ 200 neurons per condition monitored. Scale bar: 40 μ m. One-way ANOVA Tukey's multiple comparisons test, $n = 3$, data presented as mean \pm SE, ** $P = 0.004$.

3-positive cells in the spinal cord of SOD1^{G93A} mice, compared to injection with AAV9-GFP (Fig 7C and D)(mean: AAV9-GFP 84.44 ± 1.47%; AAV9-GFP-50aa 73.24 ± 0.39%). Additionally, the number of NeuN-positive cells in the ventral horn of the spinal cord was significantly higher in the 50 aa-injected group compared with GFP control (Fig 7E) (mean: AAV9-GFP 1 ± 0.12 AAV9-GFP-50aa 1.37 ± 0.12).

Taken together, our *in vivo* and *in vitro* data demonstrate that a CRMP4-dynein complex contribute to motor neuron loss in ALS disease. Importantly, this process is reversible and can be prevented by blocking the CRMP4 and dynein interaction.

Discussion

Duplan *et al* (2010) previously reported that CRMP4 is elevated in SOD1^{G93A} MNs both *in vivo* and *in vitro* and lead to their loss. By reducing CRMP4 levels, the group demonstrated protective effect on MN health (Duplan *et al*, 2010). However, the mechanism by which CRMP4 mediates MN toxicity, its involvement in other ALS models, and its relevance to human ALS disease were unknown. In this work, we discover subcellular alterations in CRMP4 levels in sALS human patients, in C9orf72 human-derived MNs, and in the SOD1^{G93A} mice CRMP4 alterations dependent on dynein activity. Specifically, CRMP4-dynein interactions are mediated by amino acids 100–150 in the CRMP4 protein, a region in which mutation was indeed correlated with ALS (Blasco *et al*, 2013). Notably, CRMP4-dynein complexes are enriched in ALS-diseased MNs and lead to ~25% cell death observed in ALS-diseased spinal cord. Finally, we show that blocking the CRMP4-dynein interaction rescued this MN population, both *in vitro* and *in vivo* (Fig 7F). These results pose many important open questions:

What is the cause for CRMP4 alterations in ALS-diseased MN axons?

Here, we reported that CRMP4 is elevated in the soma of several ALS model MNs but is decreased near distal axons. We further demonstrated that *Sema3A* facilitates an increase in CRMP4 protein levels specifically in ALS-diseased MN somata and proximal axons. Since in our previous report we demonstrated that ALS disease muscles secrete *Sema3A*, we assume that CRMP4 elevations in

somata and proximal axons are due to the nearby presence of *Sema3A*. However, the mechanism responsible for the permanent elevation of CRMP4 specifically in ALS-diseased MNs is unknown. miRNA downregulation and defects in local protein synthesis are common features in several ALS models (Haramati *et al*, 2010; Costa & Willis, 2018). Along with that, *Sema3A* was shown to induce axonal local synthesis in several neuronal systems (Campbell & Holt, 2001; Wu *et al*, 2005; Manns *et al*, 2012; Cagnetta *et al*, 2018, 2019). Thus, we hypothesize that the permanent elevation in CRMP4 that we observed in diseased MN somata and proximal axons are possibly due to increase in axonal protein synthesis. Specifically, our recent published work suggests that miR126-5p is downregulated in both muscles and MN axons in several ALS models (Rotem *et al*, 2017; Maimon *et al*, 2018). Thus, it is tempting to speculate further that miR126-5p downregulation mediates CRMP4 increases in ALS-diseased MNs via local protein synthesis and consolidation of retrograde death signals in ALS models. Another possibility for CRMP4 alterations in ALS disease is a proteolytic degradation of CRMP4 at the injured site of the neuron, as has been shown before (Jang *et al*, 2010). Further experiments are needed to test the probability of those ideas.

How does CRMP4-dynein activate caspase 3 in ALS-diseased MNs?

Our data further suggest that CRMP4 forms complexes with dynein along ALS-diseased MNs and leads to their loss via a caspase 3-dependent cascade. However, it is still not clear whether CRMP4 itself activates the apoptotic program or whether it plays a regulatory role in recruiting the death complex. Since CRMP members have not yet been reported to act as transcription factors, we assume that CRMP4 is a critical part of a retrograde signaling complex that might contain additional proteins. For example, DLK regulation of JNK and c-Jun might also be a part of this death signal mediated by *Sema3A* in ALS MNs, since it was previously shown that both DLK and JNK signaling are elevated in ALS models and that they are part of a retrograde death signal (Perlson *et al*, 2010; Sengupta Ghosh *et al*, 2011; Siu *et al*, 2018; Escudero *et al*, 2019). Another possibility is that the neurotrophic receptor p75^{NTR} is also involved in this process. p75^{NTR} regulates a diverse range of cellular functions including axon pruning (Singh *et al*, 2008) and neuronal death (Bamji *et al*, 1998; Kenchappa *et al*, 2010; Pathak *et al*, 2018).

Figure 7. Blocking the formation of the CRMP4-dynein complexes reduces motor neuron toxicity *in vivo*.

- Representative images and insets of WT and SOD1^{G93A} SC cross sections at P90. Blue: denotes DAPI, Red: denoted NeuN, and White: denotes activated caspase 3. Scale bar: 20 μm.
- Quantification of active caspase 3-positive cells in P90 WT and SOD1^{G93A} SC. 3 different mice in each condition analyzed. We monitored active caspase 3 expression in total of 108 cells in WT SC and 123 cells in SOD1^{G93A}. Student's *t*-test, *n* = 3, data presented as mean ± SE, *****P* < 0.0001.
- Representative images of P90 SOD1^{G93A} mice SC cross sections that were injected with AAV9-GFP/AAV9-50aa-GFP. Blue: denotes DAPI, Red: denoted NeuN, and White: denotes activated caspase 3. Scale bar: 10 μm.
- Quantification of caspase 3-positive cells in P90 SOD1^{G93A} mice SC cross sections that were injected with either AAV9-GFP or AAV9-50aa-GFP. Data collected from 3 different mice in each condition. We monitored active caspase 3 expression in total of 228 cells in P90 SOD1^{G93A} mice SC cross sections that were injected with AAV9-GFP and 179 cells P90 SOD1^{G93A} mice SC cross sections that were injected with AAV9-50aa-GFP. Student's *t*-test, *n* = 3, data presented as mean ± SE, ***P* = 0.0019.
- Quantification of the number of NeuN-positive cells in P90 SOD1^{G93A} mice SC cross sections that were injected with either AAV9-GFP or AAV9-50aa-GFP. Data collected from 3 different mice in each condition. We monitored the number of NeuN-positive cells from total of 228 cells in P90 SOD1^{G93A} mice SC cross sections that were injected with AAV9-GFP and 179 cells P90 SOD1^{G93A} mice SC cross sections that were injected with AAV9-50aa-GFP. Unpaired *t*-test with Welch's correction, *n* = 3, data presented as mean ± SE, **P* = 0.0484.
- Working model—CRMP4-dynein complex formation is enhanced in ALS disease and leads to subtype-specific neuronal loss.

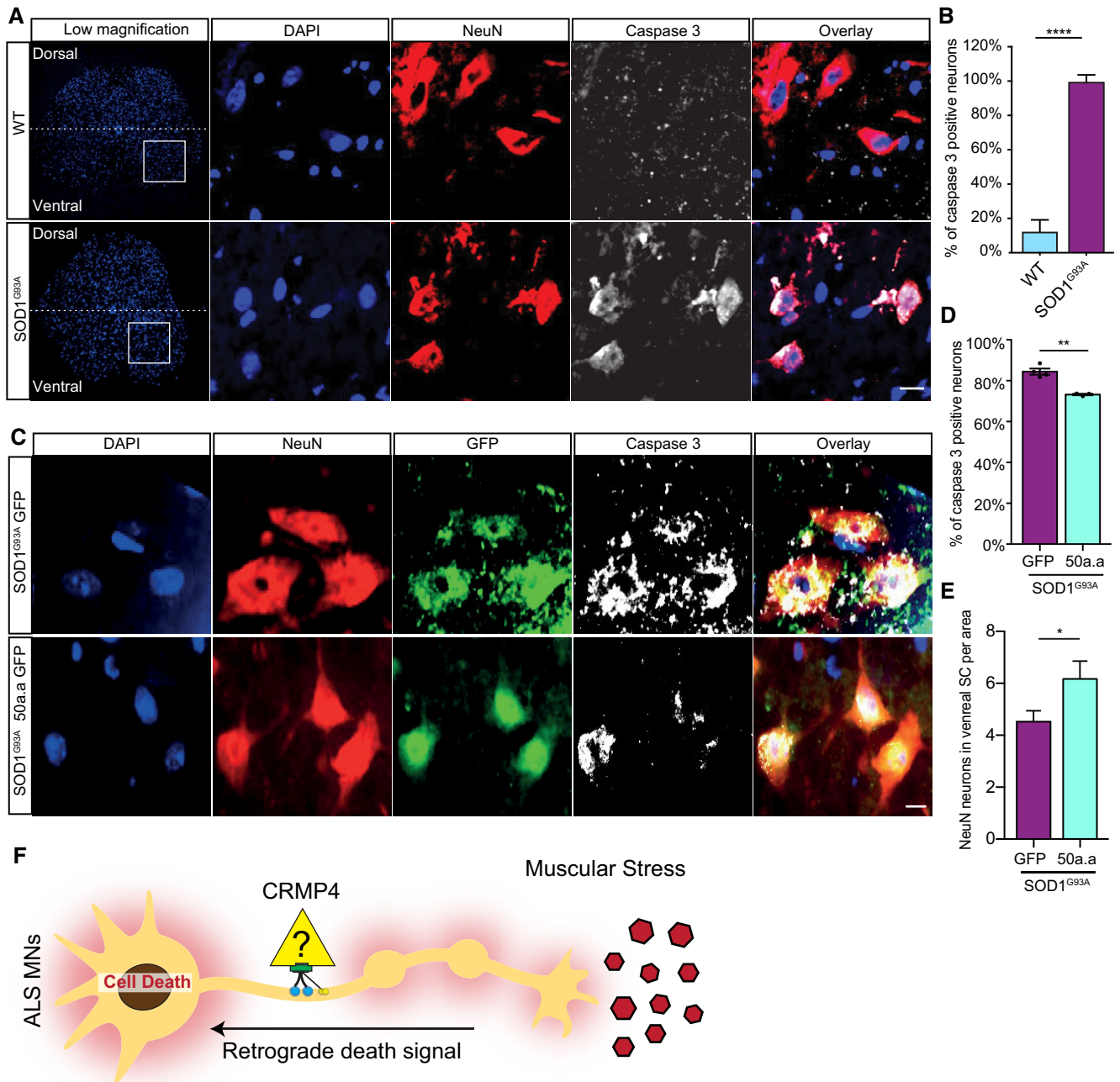


Figure 7.

p75^{NTR} is retrogradely transported along the axon (Deinhardt *et al*, 2006; Harrington & Ginty, 2013; Cosker & Segal, 2014) and plays a role in generating a retrograde apoptotic signal that activates JNK (Kenchappa *et al*, 2010). It is noteworthy that the activity of Sema3A and its receptor was previously linked to p75^{NTR} (Ben-Zvi *et al*, 2007). Another possible candidate that was shown to be coupled with Sema3A is PTEN (Chadborn *et al*, 2006). Furthermore, it was established that the p75^{NTR}-dependent apoptosis signal is promoted by PTEN activation (Song *et al*, 2010). Thus, future experiments should examine whether PTEN, p75^{NTR}, and JNK indeed participate in Sema3A-dependent retrograde death signals in ALS.

CRMP4 gain of toxicity in ALS disease

CRMP4 overexpression has been suggested to cause MN death in ALS models (Charrier *et al*, 2003; Duplan *et al*, 2010). Furthermore, a *CRMP4* mutation was associated with ALS in patients (Blasco *et al*, 2013). However, the mechanism of CRMP4 toxicity in ALS MNs is unknown. Here, we demonstrate a specific mechanism by which CRMP4 toxicity to MNs is dependent on dynein activity. Moreover, we demonstrate that amino acids 100–150 of CRMP4 are responsible for the CRMP4 and dynein interaction. Importantly, the ALS-associated mutation in CRMP4 is located in this motif. Our data

show a stronger dynein interaction for the mutant CRMP4, which is in accordance with CRMP4 gain of toxicity. Alternatively, CRMP4 has been documented before, in a number of experimental models to elevate post-neuronal injury (near injury site). Thus, it is possible that the results in this manuscript reflect a response of motor neurons to stress rather than an ALS-specific mechanism (Jang *et al*, 2010). Additional studies will be needed to dissect in detail the mutant CRMP4 activity in ALS-diseased MNs.

Materials and Methods

Animals

SOD1^{G93A} (Stock No. 002726) mice were originally obtained from Jackson Laboratories and maintained by breeding with C57BL/6J mice.

B6;129S6-ChAT^{tm2(cre)Low1}/J (Stock No. 006410) and B6;129S6Gt (ROSA)26 Sor^{tm14(CAG-tdTomato)Hze}/J (Stock No. 007908) mice were originally obtained from Jackson Laboratories. Animals were cross-bred in the Tel-Aviv SPF animal unit to yield homozygous ChAT::Rosa^{tdTomato} mice. The ChAT::Rosa^{tdTomato} colony was maintained by in-breeding males and females from the colony. The ChAT::Rosa^{tdTomato} colony was cross-bred with SOD1^{G93A} to yield SOD1^{G93A/ChAT::tdTomato} mice. C57BL/6J mice were used as a WT mouse strain. Mice were genotyped using the PCR (KAPA Bio Systems—Wilmington, MA, USA). DNA samples were generated from mouse ear or tail. Animal experiments were performed under the supervision and approval of the Tel-Aviv University Committee for Animal Ethics.

iPSC cultures

Healthy/Control iPSC lines, provided by Dr. Sami Barmada, were created and characterized as before (Tank *et al*, 2018). Two lines from fALS patients carrying the C9orf72 mutation, and two lines from healthy controls, were used for all experiments.

Name	Age donated	Age of onset	Gender	
ALS883	51	49 (Lumbar)	M	(> 44 repeats) per Athena 7/26/2012
ALS312	54	52 (Lumbar)	M	(44 and 2 repeats) by Athena Diagnostics 10/03/2012
Control746	58		M	Healthy
Control1021	54		F	Healthy

Colonies were groomed daily until each well of the 6-well plate was between 30 and 40% confluence and no spontaneously differentiated cells were observed. At this point, we used the direct iMN (diMN) differentiation in monolayers from hiPSCs protocol published by Cedar Sinai and approved by Dhruv Sareen (protocol number: CSMNC-SOP-C-005) for our experiments. Briefly, we induced MN differentiation by MN Differentiation Stage 1 media: prepared with—IMDM (LifeTech), F12 (LifeTech), NEAA (Gibco), B27 (LifeTech), N2 (LifeTech), PSA (LifeTech), LDN193189 0.2 μM (Selleck), SB431542 10 μM (Tocris), and CHIR99021 3 μM (Cayman

Chemicals). The media was gently added to the wells, and colonies were grown with it for 5 days. MN differentiation Stage 2: At day 6, the colonies were dissociated, using Accutase, and 100K cells were plated in the proximal compartment of our micro fluidic device. Stage 2 media, which contains IMDM, F12, NEAA, B27, N2, PSA, LDN193189 0.2 μM (Selleck), SB431542 10 μM (Tocris), and CHIR99021 3 μM (Cayman Chemicals), All-trans RA 0.1 μM (Stemgent), and SAG 1 μM (Sonic Hedgehog Agonist—Cayman Chemicals) media was added to both the distal and proximal compartments of the MFC and refreshed every 2 days until day 11. MN differentiation Stage 3: At day 12 the media was changed to stage 3 media prepared with IMDM, F12, NEAA, B27, N2, PSA, Compound E 0.1 μM (Calbiochem), DAPT 2.5 μM (Cayman Chemicals), db-cAMP 0.1 μM (Millipore), All-trans RA 0.5 μM (Stemgent), SAG 0.1 μM, ascorbic acid 200 ng/ml (Sigma), BDNF 10 ng/ml (Alomone Labs), and GDNF 10 ng/ml (Alomone Labs) and was refreshed every 2 days until cells exhibited MN neuronal morphology and positive markers. Human iPSC experiments were performed under the supervision and approval of the Tel-Aviv University Committee for Human Ethics.

Microfluidic chamber preparation

Polydimethylsiloxane (PDMS) microfluidic chambers (MFCs) were designed and cast as described previously (Ionescu *et al*, 2016). Briefly, MFCs were fabricated from our designed templates and made from PDMS mixture at 70°C. After the wells were punched, a small “cave” was made in the explant well near the grooves using a 25G needle, keeping the explant in place. Microfluidic devices were cleaned of surface particles using adhesive tape and were sterilized in 70% ethanol for 15 min. Devices were completely dried under sterile conditions using UV radiation, attached to a sterile 60-mm plastic dishes (Nunc) with gentle pressure and margins were sealed with PDMS before incubation at 60°C for 30 min to prevent the chamber from detaching. The wells and channels were filled with 150 μl of 1.5 ng/ml polyornithine (P-8638, Sigma) in PBS overnight and then replaced with 150 μl laminin (L-2020, Sigma), 1:333 in deionized distilled water (DDW) overnight. One day before plating the spinal cord explant, laminin was replaced with explant medium containing Neurobasal (Life Technologies) supplemented with 2% B27 (Invitrogen), 1% penicillin–streptomycin (Biological Industries), 1% Glutamax (Life Technologies), and 25 ng/ml brain-derived neurotrophic factor (Alomone Labs), until the day on which co-culturing began.

Motor neuron cell culture

Primary spinal cord neurons were cultured using E12.5 mouse embryos of either sex as previously described (Zahavi *et al*, 2015). Briefly, spinal cords were excised, trypsinized, and triturated. Supernatant was collected and centrifuged through a 4% BSA cushion. The pellet was resuspended and centrifuged through an Optiprep gradient (10.4% Optiprep (Sigma-Aldrich), 10 mM Tricine, 4% glucose) for 20 min at 760 g with the brake turned off. Cells were collected from the interface, washed once in complete medium, and then plated in coated growth chambers. Cells were maintained in complete neurobasal medium (Gibco) containing B27 (Gibco), 10% (v/v) horse serum (Biological Industries), 25 nM beta-mercaptoethanol, 1% penicillin–streptomycin (PS; Biological

Industries), and 1% GlutaMAX (Gibco) supplemented with 1 ng/ml glial-derived neurotrophic factor (GDNF), 0.5 ng/ml ciliary neurotrophic factor (CNTF), and 1 ng/ml brain-derived neurotrophic factor (BDNF) (Alomone Labs). Prior to plating, growth plates were coated with 1.5 g/ml poly D-L-ornithine (PLO; Sigma-Aldrich) overnight at 37°C and with 3 µg/ml Laminin (Sigma-Aldrich) for 2 h at 37°C. For immunofluorescence staining, 10,000 cells were plated on cover slides in 24-well plates. Cells were grown at 37°C in 5% CO₂.

Spinal cord explants

Spinal cords were dissected from E12.5 mouse embryos of both sexes, either using HB9::GFP or SOD1^{G93A} stripped of meninges and dorsal root ganglia. The ventral horn was separated from the dorsal horn by longitudinal cuts along the spinal cord, and transverse sections up to 1 mm were placed in the explant well. Prior to plating, growth chambers were coated with 1.5 g/ml PLO overnight at 37°C and 3 µg/ml Laminin overnight at 37°C. Explants were maintained in spinal cord explant medium containing Neurobasal, 2% B27, 1% PS, and 1% GlutaMAX, supplemented with 25 ng/ml BDNF. Explants were grown at 37°C in 5% CO₂.

Fluorescence microscopy and image analysis

All confocal images were captured using a Nikon Ti microscope equipped with a Yokogawa CSU X-1 spinning disk and an Andor iXon897 EMCCD camera controlled by Andor IQ3 software. All live-imaging assays were performed in a humidified incubation chamber at 37°C, 5% CO₂. Images were analyzed using ImageJ software.

Retrograde labeling of cell bodies in the MFC

Alexa Fluor 647-conjugated cholera toxin subunit B (CTX; Thermo Fisher C-347777) at 500 ng/ml was applied to the distal compartment of an MFC system while maintaining a higher liquid volume in the proximal compartment to prevent unspecific labeling by diffusion. After 8 h, only somata whose axons traversed to the distal compartment were labeled.

Recombinant Sema3A application

Recombinant Sema3A (R&D, 1250-S3-025) at 500 ng/ml was used in our experiments. We dilute the Sema3A in poor neurobasal (PNB) containing Neurobasal medium (Gibco) with 1% PS and 1% Glutamax.

Retrograde transport inhibition

In order to inhibit dynein-dependent retrograde transport, Cillibrevin-D (Merck-Millipore, 250401) at 10 µM was applied to the distal compartment of the MFC while maintaining a proximal-to-distal volume gradient.

Inhibition of dynamin-dependent endocytosis

Dynasore (Sigma-Aldrich, D7693) at 100nM was added to the distal compartment of the MFC while maintaining a proximal-to-distal volume gradient.

Pull-down assays

For the cell cultures pull-down experiments, 2 × 10⁶ COS7 cells were plated in 10 cm culture dishes. The following day, cells were transfected using calcium phosphate protocol with Flag-CRMP4/GFP-CRMP4/ GFP-Delta-CRMP4/Mutated-Flag-CRMP4/AAV9-GFP/AAV9-GFP-50aa vector. The next day, cells were lysed, and proteins were extracted using lysis buffer containing PBS, 1% Triton X-100, and 1% protease, and phosphatase inhibitors (Roche), followed by centrifugation and collection of the supernatant. At this point, immunoprecipitation preparation of the lysate was precleared with protein A agarose beads (Roche). Following overnight incubation with primary anti-flag antibody/anti-DIC antibody, complexes were incubated with protein A agarose beads for 2 h at 4°C and then precipitated and washed with PBS with 0.1% Triton X-100 (Sigma). Proteins were eluted by boiling in sample buffer and then subjected to western blot precipitation analysis with CRMP4/dynactin p150/Flag antibody (Sigma-Aldrich F3165)/DIC. We used mouse IgG antibody as a control (SC-2025). For sciatic nerve pull downs, 12 sciatic nerves were pooled for each experiment. Here as well, the P90 sciatic nerve samples were first excised and homogenized in lysis buffer containing PBS and 1% protease and phosphatase inhibitors (Roche), followed by centrifugation and collection of the supernatant. Then, we performed the pull-down assay using the technique described above. Under these conditions, pull downs were performed using DIC (Millipore MAB1618) and CRMP4 (Millipore AB5454) antibodies.

Western blotting

Sciatic nerve axoplasm was isolated by excising and cutting sciatic nerves into short segments, followed by detergent-free buffer homogenized with PBS X1 protease and phosphatase inhibitors (Roche), followed by centrifugation and collection of the supernatant. Complete sciatic nerve extracts were achieved in the same manner with the exception of adding 1% Triton X-100. The protein concentration was determined using the Bio-Rad Protein Assay. Protein samples were denatured by boiling in SDS sample buffer and then electrophoresed in 8% polyacrylamide gels (SDS-PAGE). Proteins were transferred to a nitrocellulose membrane and then immunoblotted with appropriate primary antibodies: anti-CRMP4—1:2,000 (Millipore AB5454), anti-DIC—1:1,000 (Millipore MAB1618), anti-p150 1:250 (BD Bioscience 611003), anti-Flag 1:4,000 (Sigma-Aldrich F3165), anti-Tubulin 1:10,000 (ab7291), and anti-tERK 1:10,000 (M5670), diluted in 5% (w/v) skim milk (BD Difco) in TBS-T, followed by species-specific HRP-conjugated secondary antibodies (Jackson Laboratories) and visualized using a myECL imager (Thermo), according to the manufacturer's instructions. ImageJ software was used for quantification.

AAV production

We used AAV serotype 9 (AAV9) for overexpression experiments. The AAV9 produced in AAVpro 293T cells (Takara-Clontech, #632273), with the AAVpro[®] Purification Kit (All Serotypes) from TaKaRa (#6666). For each construct four 15-cm plates were transfected with 20 µg of DNA (AAVplasmid containing the construct of interest and two AAV9 helper plasmids) using jetPEITM

(Polyplus-transfection) in DMEM medium without serum or antibiotics. pAdDeltaF6 and pPHP.S helper vectors were kind gift from Prof. Fainzilber. Medium (DMEM, 20% FBS, 1 mM sodium pyruvate, 100 U/ml penicillin, 100 mg/ml streptomycin) was added on the following day to a final concentration of 10% FBS, and extraction was done at 3 days post-transfection. Purification was performed according to the manufacturer's instructions. For all constructs, we obtained titers in the range of 10^{13} – 10^{14} viral genomes/ml.

Vector injections

The injection procedure was performed on pre-symptomatic ~ P60 mice. Mice were first anesthetized using a mixture of xylazine and ketamine. Then, a thin incision was performed in the mouse skin in order to expose the area of the L5 and L6 vertebrae. Next, 5 μ l of AAV9-GFP (6.5×10^{14} vg/ml) or AAV-GFP-50aa (1.21×10^{13} vg/ml) were injected by intrathecal injection to L5–L6 vertebrae in the spinal cord using a 25 μ l Hamilton syringe and a 30G Hamilton needle. All animal experimentations were approved by the Tel-Aviv University Animal Ethics Committee. This method was conducted with the help of Dr. Michael Tolmasov. All the tissues were taken 4 weeks post-injection.

Human muscle biopsy for intra-muscular nerve staining

Intra-muscular nerve staining was performed on muscle biopsies from ALS patients and non-ALS patients. All clinical and muscle biopsy materials used in this study were obtained with written informed consent during 2016–2020 for diagnostic purposes followed by research application, approved by the institutional review board. Deltoid, quadriceps, or gastrocnemius skeletal muscle samples were excised via open biopsies, and pathological analysis was performed at the neuromuscular pathology laboratory at Sheba Medical Center, Ramat Gan, Israel. All ALS patients were diagnosed with clinically definite or probable ALS according to Awaji criteria (de Carvalho *et al*, 2008) Control muscles included a variation of findings, which were consistent with a diagnosis of normal muscle, severe, chronic ongoing denervation and reinnervation due to spinal stenosis, necrotic autoimmune myopathy, type 2 fiber atrophy due to disuse, and overlap myositis syndrome.

Frozen muscle biopsies were cryo-sectioned to 10 μ m thick slices, mounted onto slides, and air dried for 30 min in room temperature (RT). Sections were washed in PBS, fixed in 4% PFA for 20 min, and permeabilized with 0.1% Triton, and blocked with 5% goat serum (Jackson Laboratories) and 1 mg/ml BSA (Amresco). Sections were then incubated with appropriate antibodies overnight at 4°C in blocking solution Rabbit anti-CRMP4 (Millipore AB5454, 1:250), Chicken anti-NFH (Abcam, 1:1,000). Sections were washed again and incubated for 2 h with secondary antibodies (1:1,000, Jackson Laboratories and Thermo Fisher), washed, and mounted with ProLong Gold (Life Technologies).

IHC of CRMP4 in human spinal cord tissue

The Dako Autostainer Link 48 (Agilent, USA) was used for all human spinal cord immunohistochemistry. The CRMP4 antibody (Millipore AB5454) was used at 1:700 for 30 min at room temperature. Heat-induced epitope retrieval was used prior to staining with Dako's EnV

Flex Low pH TRS. The Dako Envision Flex Plus Mouse Link Kit (Agilent, USA) to detect the antibody along with the Dako DAB (Agilent, USA). CRMP4 relative expression was semi-quantified by scoring IHC spinal cord sections between 1 and 3, blindly: 1 = low expression, 2 = middle expression, and 3 = high expression.

Sciatic nerve sectioning and immunostaining

Sciatic nerves of P90 mice were isolated and immediately fixed by using 4% PFA followed by 20% sucrose incubation. Then, the samples were embedded by freezing in Tissue-Tek[®] OCT. Next, 10 μ m lumbar sciatic nerve sections were prepared using Cryotome[™] FSE cryostat (Thermo Fisher Scientific). Sections were rinsed in PBS and then permeabilized with 0.1% Triton X-100, 5% Goat Serum (GS), 1 mg/ml bovine serum albumin IgG, and protease free (BSA) in PBS. Primary antibodies against NFH 1:500 (Abcam ab72996/ Covance smi31p/ Covance smi32p)/CRMP4 1:400 (Millipore AB5454)/GFP 1:400 (Abcam ab13970) were diluted in blocking solution, 5% GS, 1 mg/ml BSA in PBS, and incubated overnight at 4°C. Samples were incubated with species-specific fluorescent secondary antibodies for 2 h at room temperature. ProLong antifade medium (Molecular Probes) was added, and the samples were covered with a #1.5, 18 \times 18 mm cover slide.

Spinal cord sectioning and immunostaining

Spinal cord of P90 mice was isolated and immediately fixed by using 4% PFA followed by 20% sucrose incubation. Then, the samples were embedded by freezing in TissueTek[®] OCT. Next, 10 μ m lumbar spinal cord sections were prepared using Cryotome[™] FSE cryostat (Thermo Fisher Scientific). Sections were rinsed in PBS and then permeabilized with 0.1% Triton X-100, 5% Goat Serum (GS), 1 mg/ml bovine serum albumin IgG, and protease free (BSA) in PBS. Primary antibodies against NeuN 1:500 (Millipore MAB377)/CRMP4 1:400 (Millipore AB5454)/GFP 1:400 (Abcam ab13970)/activated Caspase 3 1:15 (Biovision 3015-100) were diluted in blocking solution, 5% GS, 1 mg/ml BSA in PBS, and incubated overnight at 4°C. Samples were incubated with species-specific fluorescent secondary antibodies for 2 h at room temperature. ProLong antifade medium with Dapi (Molecular Probes) was added, and the samples were covered with a #1.5, 18 \times 18 mm cover slide.

Immunostaining of cell cultures

Cultures were fixed in 4% paraformaldehyde and permeabilized with 0.1% Triton X-100, 5% GS, 1 mg/ml BSA in PBS. Samples were blocked for 1 h with blocking medium containing 5% GS and 1 mg/ml BSA in PBS. Primary antibodies against Tau 1:100 (abcam, ab80579) NFH-1:500 (Sigma-Aldrich N4142), PlexinA1-1:100 (Alomone lab, APR-081-F), CRMP4-1:100 (Millipore, AB5454), GAPDH 1:500 (abcam, ab9484), Tubulin 1:500 (abcam, ab7291), HB9 1:100 (IMGEX, IMG-6549A) were diluted in blocking solution and incubated overnight at 4°C. Samples were incubated with species-specific fluorescent secondary antibodies for 2 h at room temperature. For visualizing nuclei in myotubes, DAPI was used. In the MFC, after the staining protocol was completed, the MFC was peeled from the dish by gently pulling it from the proximal to the distal side.

Whole mount NMJ immunofluorescence staining

Gastrocnemius muscles of P60/P90 SOD1^{G93A/ChAT::tdTomato} or WT^{ChAT::tdTomato} mice were dissected from mice, washed with cold PBS, and cut in longitudinal sections along the fiber before fixed in 4% paraformaldehyde (PFA) in PBS for 15 min at room temperature, while rocking. From fixation until the end of staining protocol (mounting), muscle fibers were washed three times with PBS after each step, except between blocking and primary antibodies staining. After been fixated, muscle fibers were further dissected into smaller section, along fiber orientation. For postsynaptic AChR labeling, the fibers were then stained with α BTX (TMR- α -bungarotoxin; T0195 Sigma) 2 μ g/ml in PBS for 15min at RT while rocking. Fibers were then permeabilized in -20°C methanol for 5min, then blocked for 1 h at RT with blocking solution (2% BSA, 0.4% Triton X-100 in PBS), followed by the application of primary antibodies diluted in blocking solution; NFH (1:500; ab72996, Abcam) and CRMP4 (1:250; Millipore, AB5454) and incubation overnight at RT while rocking. On the next day, samples were incubated with species-specific fluorescent secondary antibodies for 4 h at room temperature while rocking. Muscle fibers were then placed on a cover slide suitable for imaging, mounted with Vectashield (Vector Laboratories) and sealed with clear nail polish. Slides were kept in RT until completely dried, then stored at 4°C until imaged in the microscope.

Proximity ligation assay

The proximity ligation assay (PLA) was used to visualize the colocalization of selected proteins; it was performed as previously described (Söderberg *et al.*, 2008). Briefly, iPSC-derived MNs and murine-MN cultures were grown in the MFC on glass dishes for 18 and 5 DIV, respectively, and were then fixed in 4% PFA, at 4°C for 20 min. Subsequently, the samples were blocked and permeabilized with 5% donkey serum, 1% BSA, and 0.1% Triton X-100 in PBS for 1h and incubated with anti-CRMP4 and anti-DIC antibodies overnight at 4°C. Interactions (range ~40 nm) were detected by the proximity ligation assay Duolink kit (Sigma: PLA probe anti-mouse minus DUO92004, anti-rabbit plus DUO92002, and the detection kit Far Red). PLA was performed according to the manufacturer's instructions. Coverslips were washed, mounted, and imaged by confocal microscopy. Half ligation samples were used as a negative control. The axonal PLA signal was quantified with ImageJ software using an axonal mask based on an endogenous mCherry/Rosa signal. The PLA puncta signal was quantified with the analyzed particle function of the software.

CRMP4-like peptide design and insertion into MNs

The Dynein-CRMP4 blocking peptide design was based on previous findings by Arimura *et al.* (2009), which pointed to 50 specific amino acid sequences responsible for CRMP2 binding to dynein (Arimura *et al.*, 2009). Peptides were prepared by Alomone labs and GL Biochem. Peptide sequences are as follows:

Name	Sequence	MW (Da)
Peptide-1	TTMIIDHVPEPE	1,480 Da
Peptide-2	SSLTEAYEKWREWADGKS	2,143 Da

Table (continued)

Name	Sequence	MW (Da)
Peptide-3	CCDYALHVDI	1,151 Da
Peptide-4	THWNDSVKQ	1,114 Da

The peptides were inserted into axons by harsh pipetting. Final concentration of 10 μ M of each peptide were inserted. Tamra peptide was generously donated by Dr. Mike Fainzilber's laboratory (10 μ M final concentration).

Vectors

CRMP4 and CRMP4 Δ 100–150 (containing deletion of the coding sequence 301–450bp) were sub-cloned in frame into the pLL3.7-GFP (Addgene) mammalian expression vector. Flag-CRMP4 and mutated Flag-CRMP4-I141V, used in the pull-down assays, was cloned into pCDNA3 vector (Invitrogen). GFP and GFP-50aa (containing the coding sequence of CRMP4 301–450 bp) were sub-cloned in frame into the pAAV-CBh (Vector Builder) mammalian gene expression vector.

Experimental design and statistical analysis

All statistical analyses were performed using GraphPad Prism v6.0. For two-group analysis, Student's *t*-test or the Mann-Whitney test was used, as determined by a normality test. For multiple comparisons, ANOVA was used with the Tukey or Holm–Sidak *post hoc* tests. All experiments include at least 3 biologically independent repeats; Significance was set at $P < 0.05$.

Ethics approval and consent to participate

Animal experiments were performed under the supervision and approval of the Tel-Aviv University Committee for Animal Ethics. Human iPSC experiments were performed under the supervision and approval of the Tel-Aviv University Committee for Human Ethics.

Data availability

This study includes no data deposited in external repositories. All data generated or analyzed during this study are included in this published article.

Expanded View for this article is available online.

Acknowledgments

This work was supported by IsrALS Foundation, the Israel Science Foundation (735/19), Ministry of Science and Technology State of Israel, and the European Research Council (grant number 309377) to E.P, Czech Health Research Council grant no. NV18-04-00085 to MB, Czech Science Foundation grant no. 21-24571S to MB and RW, and Grant Agency of the Charles University grants no. 524218 to RW. We thank Prof. Mike Fainzilber for the Tamra peptides, and help with AAV9 design. We thank Prof. Eva Feldman and Prof. Stephen Goutman for obtaining the fibroblasts for the iPSC lines. We thank Dr. Michael Tolmasov for performing the intrathecal injections. We thank Michigan Brain Bank (5P30 AG053760 University of Michigan Alzheimer's Disease Core Center) for providing patients spinal cord sections. Immunohistochemistry (IHC) was

performed at the Rogel Cancer Center Tissue and Molecular Pathology Shared Resource Laboratory (funding support: NIH P30 CA04659229).

Author contributions

Project conceptualization by RM, LA, TGP, MB, and EP; Data curation by RM, LA, TGP, TA, AI; Formal analysis by RM, LA, TGP, AI, MO, EP; Investigation by RM, LA, TGP, TA, RW, MO, ET, GA, NS, AD, SB; Methodology by RM, LA, TGP, TA, AI, RW, MO, ET, GA, NS, YA, AD, SB, MB, EP; Resource obtain from ET, GA, NS, AD, SB; Funding acquisition MB, EP; Supervision MB, EP; Writing—original draft, review and editing by RM, LA, TGP, TA, AI, YA, AD, SB, MB, EP and approved by all.

Conflict of interest

The authors declare that they have no conflict of interest point.

References

- Arimura N, Hattori A, Kimura T, Nakamuta S, Funahashi Y, Hirotsune S, Furuta K, Urano T, Toyoshima YY, Kaibuchi K (2009) CRMP-2 directly binds to cytoplasmic dynein and interferes with its activity. *J Neurochem* 111: 380–390
- Balastik M, Zhou X, Alberich-Jorda M, Weissova R, Žiak J, Pazyra-Murphy M, Cosker K, Machonova O, Kozmikova I, Chen C-H et al (2015) Prolyl isomerase Pin1 regulates axon guidance by stabilizing CRMP2A selectively in distal axons. *Cell Rep* 13: 812–828
- Bamji SX, Majdan M, Pozniak CD, Belliveau DJ, Aloyz R, Kohn J, Causing CG, Miller FD (1998) The p75 neurotrophin receptor mediates neuronal apoptosis and is essential for naturally occurring sympathetic neuron death. *J Cell Biol* 140: 911–923
- Ben-Zvi A, Ben-Gigi L, Klein H, Behar O (2007) Modulation of semaphorin3A activity by p75 neurotrophin receptor influences peripheral axon patterning. *J Neurosci* 27: 13000–13011
- Bilsland LG, Sahai E, Kelly G, Golding M, Greensmith L, Schiavo G (2010) Deficits in axonal transport precede ALS symptoms *in vivo*. *Proc Natl Acad Sci USA* 107: 20523–20528
- Blasco H, Bernard-Marissal N, Vourc'h P, Guettard YO, Sunyach C, Augereau O, Khederchah J, Mouzat K, Antar C, Gordon PH et al (2013) A rare motor neuron deleterious missense mutation in the DPYSL3 (CRMP4) gene is associated with ALS. *Hum Mutat* 34: 953–960
- Boillée S, Vande Velde C, Cleveland DW (2006) ALS: a disease of motor neurons and their nonneuronal neighbors. *Neuron* 52: 39–59
- Cagnetta R, Frese CK, Shigeoka T, Krijgsveld J, Holt CE (2018) Rapid cue-specific remodeling of the nascent axonal proteome. *Neuron* 99: 29–46.e4
- Cagnetta R, Wong HH-W, Frese CK, Mallucci GR, Krijgsveld J, Holt CE (2019) Noncanonical modulation of the eIF2 pathway controls an increase in local translation during neural wiring. *Mol Cell* 73: 474–489.e5
- Campbell DS, Holt CE (2001) Chemotropic responses of retinal growth cones mediated by rapid local protein synthesis and degradation. *Neuron* 32: 1013–1026
- de Carvalho M, Dengler R, Eisen A, England JD, Kaji R, Kimura J, Mills K, Mitsumoto H, Nodera H, Shefner J et al (2008) Electrodiagnostic criteria for diagnosis of ALS. *Clin Neurophysiol* 119: 497–503
- Castellani V, Falk J, Rougon G (2004) Semaphorin3A-induced receptor endocytosis during axon guidance responses is mediated by L1 CAM. *Mol Cell Neurosci* 26: 89–100
- Chadborn NH, Ahmed AI, Holt MR, Prinjha R, Dunn GA, Jones GE, Eickholt BJ (2006) PTEN couples Sema3A signalling to growth cone collapse. *J Cell Sci* 119: 951–957
- Charrier E, Reibel S, Rogemond V, Aguera M, Thomasset N, Honnorat J (2003) Collapsin Response Mediator Proteins (CRMPs): involvement in nervous system development and adult neurodegenerative disorders. *Mol Neurobiol* 28: 51–64
- Cosker KE, Segal RA (2014) Neuronal signaling through endocytosis. *Cold Spring Harb Perspect Biol* 6: a020669
- Costa CJ, Willis DE (2018) To the end of the line: axonal mRNA transport and local translation in health and neurodegenerative disease. *Dev Neurobiol* 78: 209–220
- De Vos KJ, Hafezparast M (2017) Neurobiology of axonal transport defects in motor neuron diseases: Opportunities for translational research? *Neurobiol Dis* 105: 283–299
- Deinhardt K, Salinas S, Verastegui C, Watson R, Worth D, Hanrahan S, Buccic C, Schiavo G (2006) Rab5 and Rab7 control endocytic sorting along the axonal retrograde transport pathway. *Neuron* 52: 293–305
- DeJesus-Hernandez M, Mackenzie I, Boeve B, Boxer A, Baker M, Rutherford N, Nicholson A, Finch NA, Flynn H, Adamson J et al (2011) Expanded GGGGCC hexanucleotide repeat in noncoding region of C9ORF72 causes chromosome 9p-linked FTD and ALS. *Neuron* 72: 245–256
- Duplan L, Bernard N, Casseron W, Dudley K, Thouvenot E, Honnorat J, Rogemond V, De Bovis B, Aebischer P, Marin P et al (2010) Collapsin response mediator protein 4a (CRMP4a) is upregulated in motoneurons of mutant SOD1 mice and can trigger motoneuron axonal degeneration and cell death. *J Neurosci* 30: 785–796
- Escudero CA, Cabeza C, Moya-Alvarado G, Maloney MT, Flores CM, Wu C, Court FA, Mobley WC, Bronfman FC (2019) c-Jun N-terminal kinase (JNK)-dependent internalization and Rab5-dependent endocytic sorting mediate long-distance retrograde neuronal death induced by axonal BDNF-p75 signaling. *Sci Rep* 9: 6070
- Firestone AJ, Weinger JS, Maldonado M, Barlan K, Langston LD, O'Donnell M, Gelfand VI, Kapoor TM, Chen JK (2012) Small-molecule inhibitors of the AAA+ ATPase motor cytoplasmic dynein. *Nature* 484: 125–129
- Fischer LR, Culver DG, Tennant P, Davis AA, Wang M, Castellano-Sanchez A, Khan J, Polak MA, Glass JD (2004) Amyotrophic lateral sclerosis is a distal axonopathy: evidence in mice and man. *Exp Neurol* 185: 232–240
- Fournier AE, Nakamura F, Kawamoto S, Goshima Y, Kalb RG, Strittmatter SM (2000) Semaphorin3a enhances endocytosis at sites of receptor–F-actin colocalization during growth cone collapse. *J Cell Biol* 149: 411–422
- Frey D, Schneider C, Xu L, Borg J, Spooren W, Caroni P (2000) Early and selective loss of neuromuscular synapse subtypes with low sprouting competence in motoneuron diseases. *J Neurosci* 20: 2534–2542
- Gershoni-Emek N, Chein M, Gluska S, Perlson E (2015) Amyotrophic lateral sclerosis as a spatiotemporal mislocalization disease: location, location, location. *Int Rev Cell Mol Biol* 315: 23–71
- Gibbs KL, Kalmar B, Rhymes ER, Fellows AD, Ahmed M, Whiting P, Davies CH, Greensmith L, Schiavo G (2018) Inhibiting p38 MAPK alpha rescues axonal retrograde transport defects in a mouse model of ALS. *Cell Death Dis* 9: 596
- Goshima Y, Nakamura F, Strittmatter P, Strittmatter SM (1995) Collapsin-induced growth cone collapse mediated by an intracellular protein related to UNC-33. *Nature* 376: 509–514
- Guedes-Dias P, Holzbaur ELF (2019) Axonal transport: driving synaptic function. *Science* 366: eaaw9997
- Haramati S, Chapnik E, Sztainberg Y, Eilam R, Zwang R, Gershoni N, McGlenn E, Heiser PW, Wills A-M, Wirguin I et al (2010) miRNA malfunction causes spinal motor neuron disease. *Proc Natl Acad Sci U S A* 107: 13111–13116
- Harrington AW, Ginty DD (2013) Long-distance retrograde neurotrophic factor signalling in neurons. *Nat Rev Neurosci* 14: 177–187

- Howard J, Hudspeth AJ, Vale RD (1989) Movement of microtubules by single kinesin molecules. *Nature* 342: 154–158
- Ionescu A, Zahavi EE, Gradus T, Ben-Yaakov K, Perlson E (2016) Compartmental microfluidic system for studying muscle–neuron communication and neuromuscular junction maintenance. *Eur J Cell Biol* 95: 69–88
- Jang SY, Shin YK, Jung J, Lee SH, Seo SY, Suh DJ, Park HT (2010) Injury-induced CRMP4 expression in adult sensory neurons; A possible target gene for ciliary neurotrophic factor. *Neurosci Lett* 485: 37–42
- Kenchappa RS, Tep C, Korade Z, Urta S, Bronfman FC, Yoon SO, Carter BD (2010) p75 neurotrophin receptor-mediated apoptosis in sympathetic neurons involves a biphasic activation of JNK and up-regulation of tumor necrosis factor- α -converting enzyme/ADAM17. *J Biol Chem* 285: 20358–20368
- LaMonte BH, Wallace KE, Holloway BA, Shelly SS, Ascaño J, Tokito M, Van Winkle T, Howland DS, Holzbaur ELF (2002) Disruption of dynein/dynactin inhibits axonal transport in motor neurons causing late-onset progressive degeneration. *Neuron* 34: 715–727
- Macia E, Ehrlich M, Massol R, Boucrot E, Brunner C, Kirchhausen T (2006) Dynasore, a cell-permeable inhibitor of dynamin. *Dev Cell* 10: 839–850
- Maimon R, Ionescu A, Bonnie A, Sweetat S, Wald-Altman S, Inbar S, Gradus T, Trotti D, Weil M, Behar O et al (2018) miR126-5p downregulation facilitates axon degeneration and NMJ disruption via a non-cell-autonomous mechanism in ALS. *J Neurosci* 38: 5478–5494
- Manns RPC, Cook GMW, Holt CE, Keynes RJ (2012) Differing semaphorin 3A concentrations trigger distinct signaling mechanisms in growth cone collapse. *J Neurosci* 32: 8554–8559
- Millecamps S, Julien J-P (2013) Axonal transport deficits and neurodegenerative diseases. *Nat Rev Neurosci* 14: 161–176
- Moloney EB, de Winter F, Verhaagen J (2014) ALS as a distal axonopathy: molecular mechanisms affecting neuromuscular junction stability in the presymptomatic stages of the disease. *Front Neurosci* 8: 252
- Munch C, Sedlmeier R, Meyer T, Homberg V, Sperfeld AD, Kurt A, Prudlo J, Peraus G, Hanemann C, Stumm G et al (2004) Point mutations of the p150 subunit of dynactin (DCTN1) gene in ALS. *Neurology* 63: 724–726
- Nagai J, Baba R, Ohshima T (2017) CRMPs function in neurons and glial cells: potential therapeutic targets for neurodegenerative diseases and CNS injury. *Mol Neurobiol* 54: 4243–4256
- Nagai J, Kitamura Y, Owada K, Yamashita N, Takei K, Goshima Y, Ohshima T (2015) Crmp4 deletion promotes recovery from spinal cord injury by neuroprotection and limited scar formation. *Sci Rep* 5: 8269
- Nicolas A, Kenna KP, Renton AE, Ticozzi N, Faghri F, Chia R, Dominov JA, Kenna BJ, Nalls MA, Keagle P et al (2018) Genome-wide analyses identify KIF5A as a novel ALS gene. *Neuron* 97: 1268–1283.e6
- Olenick MA, Dominguez R, Holzbaur ELF (2019) Dynein activator Hook1 is required for trafficking of BDNF-signaling endosomes in neurons. *J Cell Biol* 218: 220–233
- Paschal BM, Vallee RB (1987) Retrograde transport by the microtubule-associated protein MAP 1C. *Nature* 330: 181–183
- Pasinelli P, Borchelt DR, Houseweart MK, Cleveland DW, Brown RH (1998) Caspase-1 is activated in neural cells and tissue with amyotrophic lateral sclerosis-associated mutations in copper-zinc superoxide dismutase. *Proc Natl Acad Sci U S A* 95: 15763–15768
- Pathak A, Stanley EM, Hickman FE, Wallace N, Brewer B, Li D, Gluska S, Perlson E, Fuhrmann S, Akassoglou K et al (2018) Retrograde degenerative signaling mediated by the p75 neurotrophin receptor requires p150Glued deacetylation by axonal HDAC1. *Dev Cell* 46: 376–387.e7
- Perlson E, Jeong G-B, Ross JL, Dixit R, Wallace KE, Kalb RG, Holzbaur ELF (2009) A switch in retrograde signaling from survival to stress in rapid-onset neurodegeneration. *J Neurosci* 29: 9903–9917
- Perlson E, Maday S, Fu M-M, Moughamian AJ, Holzbaur ELF (2010) Retrograde axonal transport: pathways to cell death? *Trends Neurosci* 33: 335–344
- Peters OM, Ghasemi M, Brown RH (2015) Emerging mechanisms of molecular pathology in ALS. *J Clin Invest* 125: 1767–1779
- Ponnusamy R, Lebedev A, Pahlow S, Lohkamp B (2014) Crystal structure of human CRMP-4: correction of intensities for lattice-translocation disorder. *Acta Crystallogr, Sect D* 70: 1680
- Porter AG (1999) Protein translocation in apoptosis. *Trends Cell Biol* 9: 394–401
- Rahajeng J, Giridharan SSP, Naslavsky N, Caplan S (2010) Collapsin Response Mediator Protein-2 (Crmp2) regulates trafficking by linking endocytic regulatory proteins to dynein motors. *J Biol Chem* 285: 31918–31922
- Renton A, Majounie E, Waite A, Simón-Sánchez J, Rollinson S, Gibbs J, Schymick J, Laaksovirta H, van Swieten J, Myllykangas L et al (2011) A hexanucleotide repeat expansion in C9ORF72 is the cause of chromosome 9p21-linked ALS-FTD. *Neuron* 72: 257–268
- Reyes NA, Fisher JK, Austgen K, VandenBerg S, Huang EJ, Oakes SA (2010) Blocking the mitochondrial apoptotic pathway preserves motor neuron viability and function in a mouse model of amyotrophic lateral sclerosis. *J Clin Invest* 120: 3673–3679
- Rosen DR, Siddique T, Patterson D, Figlewicz DA, Sapp P, Hentati A, Donaldson D, Goto J, O'Regan JP, Deng H-X et al (1993) Mutations in Cu/Zn superoxide dismutase gene are associated with familial amyotrophic lateral sclerosis. *Nature* 362: 59–62
- Rotem N, Magen I, Ionescu A, Gershoni-Emek N, Altman T, Costa CJ, Gradus T, Pasmanik-Chor M, Willis DE, Ben-Dov IZ et al (2017) ALS along the axons – expression of coding and noncoding RNA differs in axons of ALS models. *Sci Rep* 7: 44500
- Sasaki Y, Cheng C, Uchida Y, Nakajima O, Ohshima T, Yagi T, Taniguchi M, Nakayama T, Kishida R, Kudo Y et al (2002) Fyn and Cdk5 mediate semaphorin-3A signaling, which is involved in regulation of dendrite orientation in cerebral cortex. *Neuron* 35: 907–920
- Schmidt EF, Strittmatter SM (2007) The CRMP family of proteins and their role in Sema3A signaling. In *Semaphorins: receptor and intracellular signaling mechanisms*, Pasterkamp RJ (eds), pp 1–11. New York, NY: Springer
- Sengupta Ghosh A, Wang B, Pozniak CD, Chen M, Watts RJ, Lewcock JW (2011) DLK induces developmental neuronal degeneration via selective regulation of proapoptotic JNK activity. *J Cell Biol* 194: 751–764
- Singh KK, Park KJ, Hong EJ, Kramer BM, Greenberg ME, Kaplan DR, Miller FD (2008) Developmental axon pruning mediated by BDNF-p75NTR-dependent axon degeneration. *Nat Neurosci* 11: 649–658
- Siu M, Sengupta Ghosh A, Lewcock JW (2018) Dual leucine zipper kinase inhibitors for the treatment of neurodegeneration. *J Med Chem* 61: 8078–8087
- Söderberg O, Leuchowius K-J, Gullberg M, Jarvius M, Weibrecht I, Larsson L-G, Landegren U (2008) Characterizing proteins and their interactions in cells and tissues using the in situ proximity ligation assay. *Methods* 45: 227–232
- Song W, Volosin M, Cragolini AB, Hempstead BL, Friedman WJ (2010) ProNGF induces PTEN via p75NTR to suppress Trk-mediated survival signaling in brain neurons. *J Neurosci* 30: 15608–15615
- Steinberg KM, Yu B, Koboldt DC, Mardis ER, Pamphelet R (2015) Exome sequencing of case-unaffected-parents trios reveals recessive and de novo genetic variants in sporadic ALS. *Sci Rep* 5: 9124

- Tank EM, Figueroa-Romero C, Hinder LM, Bedi K, Archbold HC, Li X, Weskamp K, Safren N, Paez-Colasante X, Pacut C *et al* (2018) Abnormal RNA stability in amyotrophic lateral sclerosis. *Nat Commun* 9: 2845
- Terenzio M, Schiavo G, Fainzilber M (2017) Compartmentalized signaling in neurons: from cell biology to neuroscience. *Neuron* 96: 667–679
- Valdez G, Tapia JC, Lichtman JW, Fox MA, Sanes JR (2012) Shared resistance to aging and ALS in neuromuscular junctions of specific muscles. *PLoS One* 7: e34640
- Wehner AB, Abdesselam H, Dickendesher TL, Imai F, Yoshida Y, Giger RJ, Pierchala BA (2016) Semaphorin 3A is a retrograde cell death signal in developing sympathetic neurons. *Development* 143: 1560–1570
- Wu KY, Hengst U, Cox LJ, Macosko EZ, Jeromin A, Urquhart ER, Jaffrey SR (2005) Local translation of RhoA regulates growth cone collapse. *Nature* 436: 1020–1024
- Yamashita N, Goshima Y (2012) Collapsin response mediator proteins regulate neuronal development and plasticity by switching their phosphorylation status. *Mol Neurobiol* 45: 234–246
- Zahavi EE, Ionescu A, Gluska S, Gradus T, Ben-Yaakov K, Perlson E (2015) A compartmentalized microfluidic neuromuscular co-culture system reveals spatial aspects of GDNF functions. *J Cell Sci* 128: 1241–1252
- Zahavi EE, Maimon R, Perlson E (2017) Spatial-specific functions in retrograde neuronal signalling. *Traffic* 18: 415–424
- Ziak J, Weissova R, Jeřábková K, Janikova M, Maimon R, Petrasek T, Pukajova B, Kleisnerova M, Wang M, Brill MS *et al* (2020) CRMP 2 mediates Sema3F-dependent axon pruning and dendritic spine remodeling. *EMBO Rep* 21: e48512



License: This is an open access article under the terms of the Creative Commons Attribution-NonCommercial-NoDerivatives License, which permits use and distribution in any medium, provided the original work is properly cited, the use is non-commercial and no modifications or adaptations are made.